R-11-11

Creep crack growth in phosphorus alloyed oxygen free copper

Rui Wu, Facredin Seitisleam
Swerea KIMAB

Rolf Sandström, Lai-Zhe Jin
Materials Science and Engineering, KTH

January 2011

Svensk Kärnbränslehantering AB
Swedish Nuclear Fuel
and Waste Management Co

Box 250, SE-101 24 Stockholm
Phone +46 8 459 84 00

ISSN 1402-3091
SKB R-11-11

Creep crack growth in phosphorus alloyed oxygen free copper

Rui Wu, Facredin Seitisleam
Swerea KIMAB

Rolf Sandström, Lai-Zhe Jin
Materials Science and Engineering, KTH

January 2011

Keywords: Creep crack growth, Compact tension, Deformation, Cavity, Microcrack, Reference stress, Phosphorus-alloyed oxygen-free copper, Interrupted.

Abstract

Using standard compact tension (CT) specimens taken from a pierce and draw cylinder, creep crack growth (CCG) has been studied in phosphorus-alloyed oxygen-free copper (Cu-OFP) parent metal at 22, 75, 175, and 215°C. Pre- and post-test metallography are performed. At higher temperatures the rupture time of CCG is shorter by a factor up of 65 than that of uniaxial at same stress/reference stress. At 175 and 215°C, crack does grow by creep about 10 mm before final instantaneous failure. In contrast, there is hardly any visible crack growth at 22 and 75°C. The tests were interrupted after 5000 to 13000 hours.

For ruptured tests at 175 and 215°C, strongly elongated and deformed grains are observed adjacent to crack. Extensive and intergranular creep cavities and microcracks are found several mm around crack. For interrupted tests at 22 and 75°C, strongly elongated and deformed grains, creep cavities, as well as microcracks are observed close to crack tip. Surface cracks from both sides have initiated and grown about 45° to the load direction towards inside.

For the interrupted tests, hardness adjacent to crack tip has more than doubled because of work hardening, or heavy deformation. This is consistent with large crack tip opening. The true strain at the crack tip is estimated to 10 and 4 for the tests at 22 and 75°C, respectively.

The stress state behind the crack tip has been modelled with FEM. Stress relaxation after loading has also been taken into account. A model for the creep damage based on the creep strain rate has been formulated that can describe the uniaxial creep rupture data without fitting parameters.

Based on the formulation for the creep damage, a model for the crack propagation has been set up. When the creep damage has reached the value unity in front of the crack tip, the crack is assumed to propagate. Taking multiaxial effects into account the observed life times of the CT specimens can be well described.

The multiaxial effects for the damage are negligible at 20 and 75ºC. However, at 175 and 215ºC the propagation rate is enhanced by up to a factor of 60, which fully explains the difference in test results between the two lowest and the two highest test temperatures.

Contents

1 Introduction

Phosphorus-alloyed oxygen-free copper (Cu-OFP) canisters with a 50 mm wall thickness are planned to be used for spent nuclear fuel in the Swedish nuclear waste programme. It is estimated that, during the first few hundred years of service, the canisters will be exposed to pressures as high as 15 MPa at a temperature up to about 100°C in the repository (Raiko et al. 2010). These conditions will cause creep deformation in the copper. Therefore, the copper canister must have sufficient creep ductility.

The copper canister will be exposed to multiaxial stress states when the external hydrostatic pressure as well as the swelling pressure from the bentonite are developed. It is well known that multiaxility can have a strong effect on the ductility of materials. Under high degrees of tensile multiaxility, ductility will decrease remarkably for notch sensitive materials, leading to premature failure. High degrees of multiaxility can be found especially at notch roots or in front of crack tips.

Cu-OFP appears the most suitable candidate canister material, owing to its good creep strength and ductility (Henderson and Sandström 1998, Seitisleam and Henderson 1997, Andersson et al. 1999, Sandström and Wu 2007). Although the creep ductility of Cu-OFP is high, a crack growing under multi-axial stress states during creep could lead to premature failure.

During the past, only limited studies of creep crack growth (CCG) under multi-axial stress state are available for copper. In 1997, CCG tests using CT specimens were conducted on a Cu-OFP (Seitisleam and Henderson 1997) at Swerea KIMAB. One specimen was tested at a reference stress of 96 MPa at 215°C without pre-existing crack, and the other at a reference stress of 120 MPa at 215°C with pre-existing crack by fatigue. Both tests were interrupted after 3800 and 6100 hours, respectively. Metallographic examinations showed that possibly some local crack growth had occurred near the notched region inside the specimens.

Another CCG test at 75°C also using CT specimen was carried out on a Cu-OFP (Andersson 2005). Only one specimen was tested. In this work, the notch with a radius of 0.15 mm was spark machined. Beginning at 121 MPa, the reference stress was successively increased to 170 MPa on the same CT specimen. Although there was a significant plasticity near the notch tip, no creep crack growth could be observed after interruption of about 6000 hours.

On cold worked copper with a high oxygen content, Auerkari *et al* carried out multi-axial creep testing using sharp notches in compact tension (CT) specimens (Auerkari et al. 2003, 2005). The creep tests at a reference stress of 46 MPa at 150°C were interrupted after 3000, 5000, 7000 and 10000 hours in order to examine the creep damage development. They did find separate intergranular creep cavities near the notch tip, in addition to a distinct grain boundary zone with elevated P content, also near the notch tip.

Recently, Auerkari and co-workers reported CCG testing results using CT specimen on a Cu-OFP friction stir weld at 175°C/34 MPa (reference stress) (Auerkari et al. 2009). After 15000 hours, the main crack started to initiate intergranular branching perpendicular to the nominal tensile principal stress. They thought that the crack initiation and branching were associated with metallurgical and defect-specific features as well as the impact of multi-axial stress state (Auerkari et al. 2009).

By using standard compact tension specimens taken from Cu-OFP, the purposes of the present project are to investigate whether Cu-OFP is sensitive to sharp notches, to examine initiation and development of creep damage around the sharp notch under multi-axial stress state, and to determine the role of creep crack growth during long term operation. Modelling of the creep crack growth is carried out using stress analysis and by formulation of function for the creep damage development.

2 Material and experiments

2.1 Material

A pierce and draw cylinder in as-received condition, having SKB internal identity T17, made of pure, oxygen-free copper doped with about 50 ppm phosphorus (Cu-OFP) is used in this study, see Figure 2-1. The thickness of the extruded cylinder is 50 mm.

Mixed grain size is observed, see Figure 2-2. The average grain size is 83 µm. The hardness (HV2) is 54.

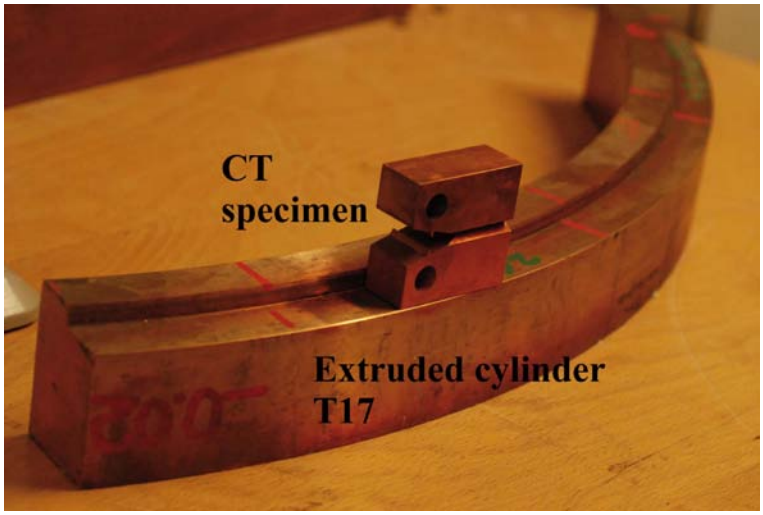

Figure 2-1. *Extruded cylinder T17 of Cu-OFP where all the compact tension (CT) specimens are extracted.*

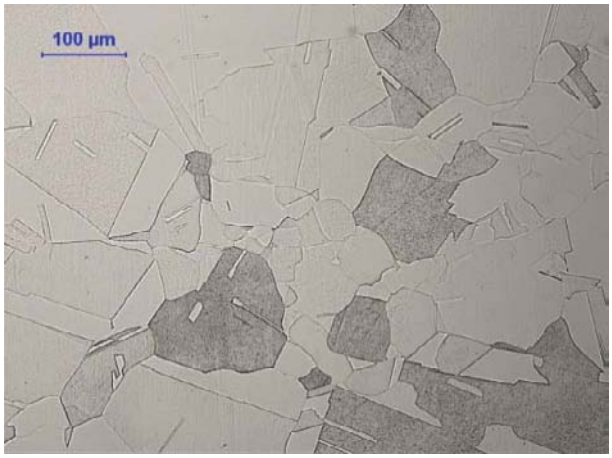

Figure 2-2. *Pierce and draw cylinder T17 of Cu-OFP where all the compact tension (CT) specimens are extracted.*

2.2 Compact tension (CT) specimen

Standard compact tension (CT) specimens with side-grooves are used for the CCG tests, see Figure 2-3. The geometry of the CT specimen having width W = 50 mm and a full thickness of B = 25 mm and a net thickness of B_N = 15 mm is given in Figure 2-4. The spark machined notch has a root radius of 0.15 mm. The notch is oriented circumferentially, which allows the crack to grow in the tangential direction, see Figure 2-1.

The exact dimensions of each CT specimen were measured prior to testing and are given in Table 2-1, together with initial reference stress σ_{ref} and initial applied load.

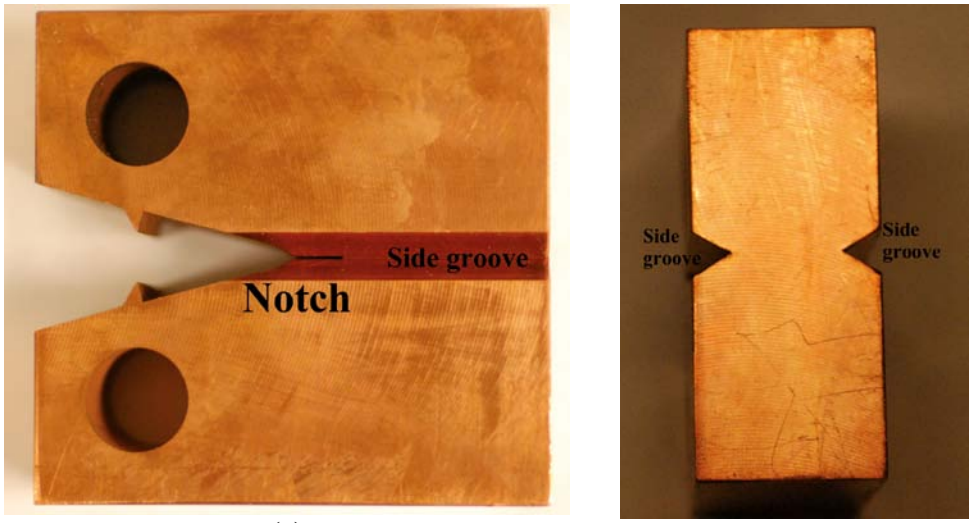

Figure 2-3. *Standard compact tension (W = 50 mm) specimen for CCG testing. (a) Side-view and (b) back-view.*

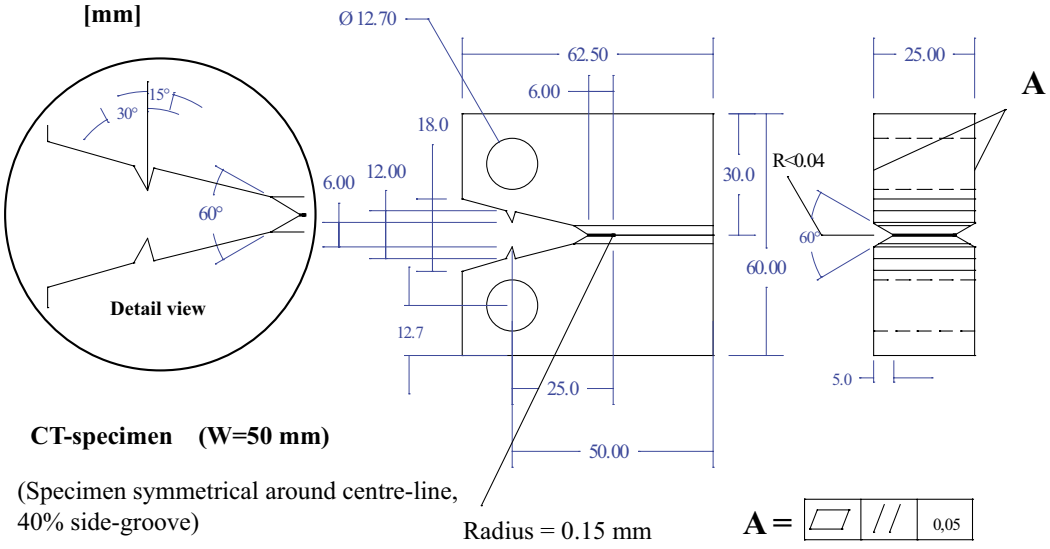

Figure 2-4. *Geometry of compact tension (CT) specimen having W = 50 mm.*

Table 2-1. CT specimen geometry, initial reference stress and initial applied load.

Specimen	W* (mm)	B_n* (mm)	B_{eq}** (mm)	a* (mm)	W-a* (mm)	Initial σ_{ref} (MPa)	Initial load (N)
CCG-215	50.562	15.245	21.188	25.622	24.94	120	11090.73
CCG-175	50.654	15.058	21.046	25.516	25.138	122.3	11405.87
CCG-75A	49.387	15.160	21.135	24.404	24.983	165	15742.62
CCG-75R	50.669	14.944	20.793	25.599	25.07	140	12814.67
CCG-22	49.454	14.971	20.979	24.405	25.049	135.5	12887.83

* Measured value

** Calculated value according to eqn. (1)

The initial load applied to the CT-specimens tested at 175 and 215°C (CCG-175 and CCG-215, respectively) is based on the relevant stress–rupture time relationship obtained from uniaxial plain creep specimens (Andersson et al. 2005, Seitisleam and Henderson 1997, Henderson and Werme 1996). The initial load applied to the CT-specimens tested at room temperature (CCG-25) and at 75°C (CCG-75 A and CCG-75R) is according to the results from higher temperature CCG tests and from Andersson (2005) and Andersson et al. (2005, 2007). The applied load is calculated using the reference stress concept. A common way of defining the reference stress in MPa (σ_{ref}) listed in Table 2-1 for a CT-specimen is given below (Miller 1988)

$$\sigma_{ref} = \frac{P}{m \cdot B_{eq} \cdot W} \tag{2-1}$$

where $$m = -(1 + \gamma(\frac{a}{W})) + \sqrt{(1+\gamma)(\gamma(\frac{a}{W})^2 + 1)} \tag{2-1a}$$

and $$B_{eq} = B - \frac{(B - B_n)^2}{B} \tag{2-1b}$$

and $$\gamma = \frac{2}{\sqrt{3}} \tag{2-1c}$$

where P is the load in N, a the crack length in mm, W the length from the centre of the load-pin hole to the back of the specimen in mm, B the width of the specimen in mm, and B_n the net thickness between the side grooves in mm. The choice of m is based on the assumption of plane stress condition. It is noted that σ_{ref} changes (increases) as the crack extends (a increases).

2.3 Creep crack growth testing

The creep crack growth (CCG) tests by means of the CT specimens follow a draft of the standard ASTM E 1457 from year 2000 (ASTM 2000). This draft has been standardised since 2007. The tests were conducted in a dead-weight lever creep test rig equipped for CCG testing. CCG test assembly is given in Figure 2-5. The direct current potential drop (PD) method was used to monitor crack progress and a purpose-built extensometer was used to measure load line displacement (LLD) or crack tip opening.

Potential drop measurements work in such a way that a constant direct current is led through the specimen across the crack propagation plane. The potential differences across the same propagation plane are then measured and recorded. As soon as crack grows, the cross section area decreases.

Under the constant current condition, the potential will increase accordingly. In ASTM E 1457 (ASTM 2000), there is an equation to calculate the crack length advance using PD recordings.

The PD method has been successfully used on various metallic materials to study crack growth (Schwalbe and Hellman 1981). However, because of the good electrical conductivity of copper, there might be difficulty in PD measurements, especially if change of PD is small. To minimise this difficulty, some considerations are taken. Firstly, a full size CT specimen with larger cross sectional area where W is equal to 50 mm is chosen. Larger cross sectional area will lead to relative large variation of PD. Secondly, for the tests at relatively lower temperature of 75°C, the CT specimen is placed in a transparent quartz chamber, see Figure 2-5. In this way, the crack growth can be visually monitored and any crack tip opening and advancing can be photographed. To measure the crack length, the surface of the CT specimen is white painted and measuring net with a vertical distance of about 1 mm is manually introduced, see Figure 2-5c. Thirdly, all the electrical contacts are protected from oxidation, which may lead to wrong data recordings.

The CT specimen is placed outside the furnace for the CCG test at 22°C, and inside the furnace for the CCG test at 175 and 215°C.

Five CCG tests have been conducted at temperatures of 22, 75, 175 and 215°C in air. The tests at the two highest temperatures progressed to rupture. The tests at 22 and 75ºC were interrupted after long time testing without any indication of failure. For two tests, the one at 22°C and another one at 75°C, the reference stress has been gradually increased in order to initiate crack propagation. The PD output, the load line displacement and temperature were periodically recorded by a logger. The maximum temperature variations with time were controlled within ±2°C of the testing temperatures. For the tests at 22 and 75°C, images of crack tip opening and crack tip appearance were regularly taken.

2.4 Post test metallography

After CCG testing, the failed/interrupted specimens are sectioned in the middle along the crack propagation direction, mounted, ground and polished to 0.25 µm, and finally etched in a solution containing 40 g CrO_3, 7.5 g HN_4Cl, 50 ml H_2SO_4, 50 ml HNO_3 and 1900 ml H_2O. Creep damage investigation around the main crack is then carried out on the etched metallographic samples using light optical microscope (LOM) and field emission gun scanning electron microscope (FEG-SEM Leo 1530).

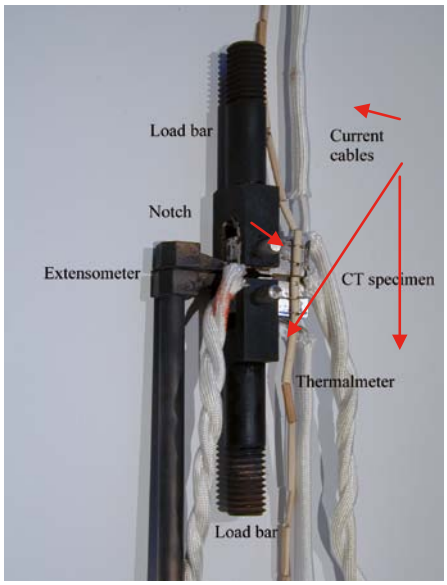

(a)

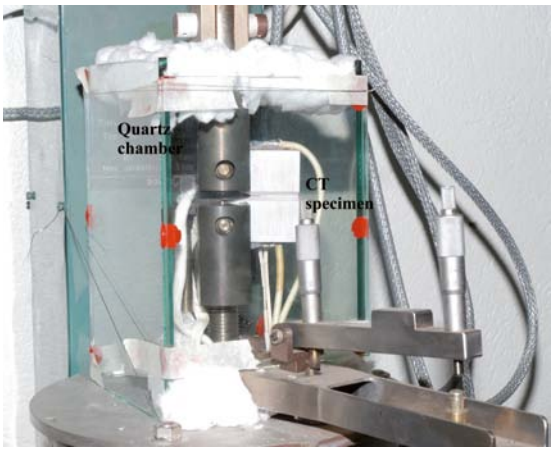

(b)

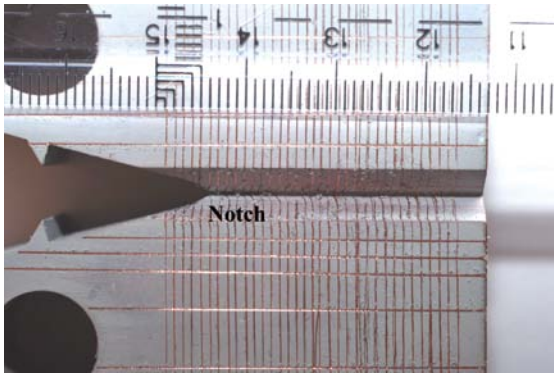

(c)

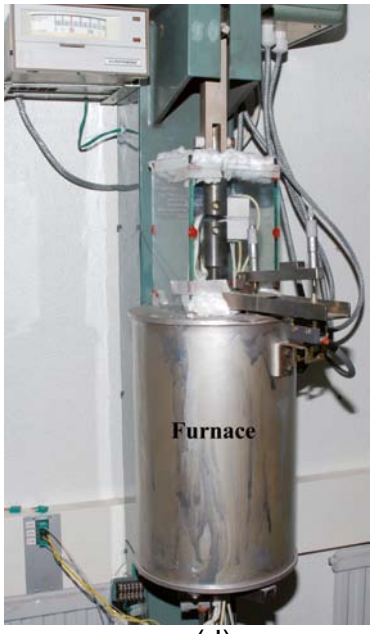

(d)

Figure 2-5. *(a) Assembly of CT specimen. This is valid for all the CCG tests. (b) – (d) For test at 75°C, white painted CT specimen with measuring net with vertical distance of about 1 mm placed in a quartz glass chamber above furnace. For test at 22°C, the CT specimen is placed outside the furnace. For tests at 175 and 215°C, the CT specimen is place inside the furnace.*

3 Results

3.1 Creep crack growth testing

CCG testing matrix and results are shown in Table 3-1. Totally, there are 5 CCG tests, 2 specimens have failed and 3 tests are interrupted. All the interrupted tests are due to unforeseen long test duration. It should be noted that loading bar arm level is readjusted once to horizontal level during uploading for the specimen CCG75A with an initial reference stress of 165 MPa. For the specimens CCG75R and CCG22, the reference stress has been gradually increased several times. The loading bar arm level is readjusted at the same time. For the tests at 175 and 215°C, there is no readjustment of the loading bar arm level.

Stress intensity factor K_I is also given for each test in Table 3-1. For CT specimens K_I is defined as (ASTM 2000)

$$K_I = \frac{P}{\sqrt{B \cdot B_N \cdot W}} \cdot \frac{2 + a/W}{(1 - a/W)^{3/2}} \cdot f(a/W) \tag{3-1}$$

where $$f(a/W) = 0.866 + 4.64(a/W) - 13.32(a/W)^2 + 14.72(a/W)^3 - 5.6(a/W)^4 \tag{3-1a}$$

Similar to the reference stress, K_I changes as the crack extends.

From Table 3-1 and Figure 3-1 it can be seen that crack tip opening (pre-LLD in Table 3-1) takes place for all tests, from about 6 mm for the specimen CCG175 to over 10 mm for the specimen CCG75A at full loading. The large crack tip opening will cause *i)* change of root radius of the notch, and *ii)* large plastic deformation or a work hardening around the crack tip.

Table 3-1. CCG testing matrix and results.

Specimen	Temp. (°C)	Reference stress σ_{ref} (MPa)	Stress intensity factor, K_I, MPa√m.	Pre-LLD under uploading (mm)	LLD under CCG (mm)	Time at rupture $t_{R,CCG}$ (h)
CCG215	215	120	24.93	5.86	13.06	121
CCG175	175	122	25.52	6.06	22.38	812
CCG75A	75	165	34.51	10.43	2.57	Interrupt. at 8925 h
CCG75R	75	140–165*	29.17–34.38	7.32	5.70	Interrupt. at 4778 h
CCG22	22	135.5–205*	28.36–42.91	6.40	15.10	Interrupt. at 13324 h

* Reference stress has been gradually increased from 140 to 165 and from 135.5 to 205 MPa for the specimen CCG75R and CCG22, respectively. Accordingly, stress intensity factor increases from 29.17 to 34.48 and from 28.36 to 42.91 MPa√m for the specimen CCG75R and CCG22, respectively.

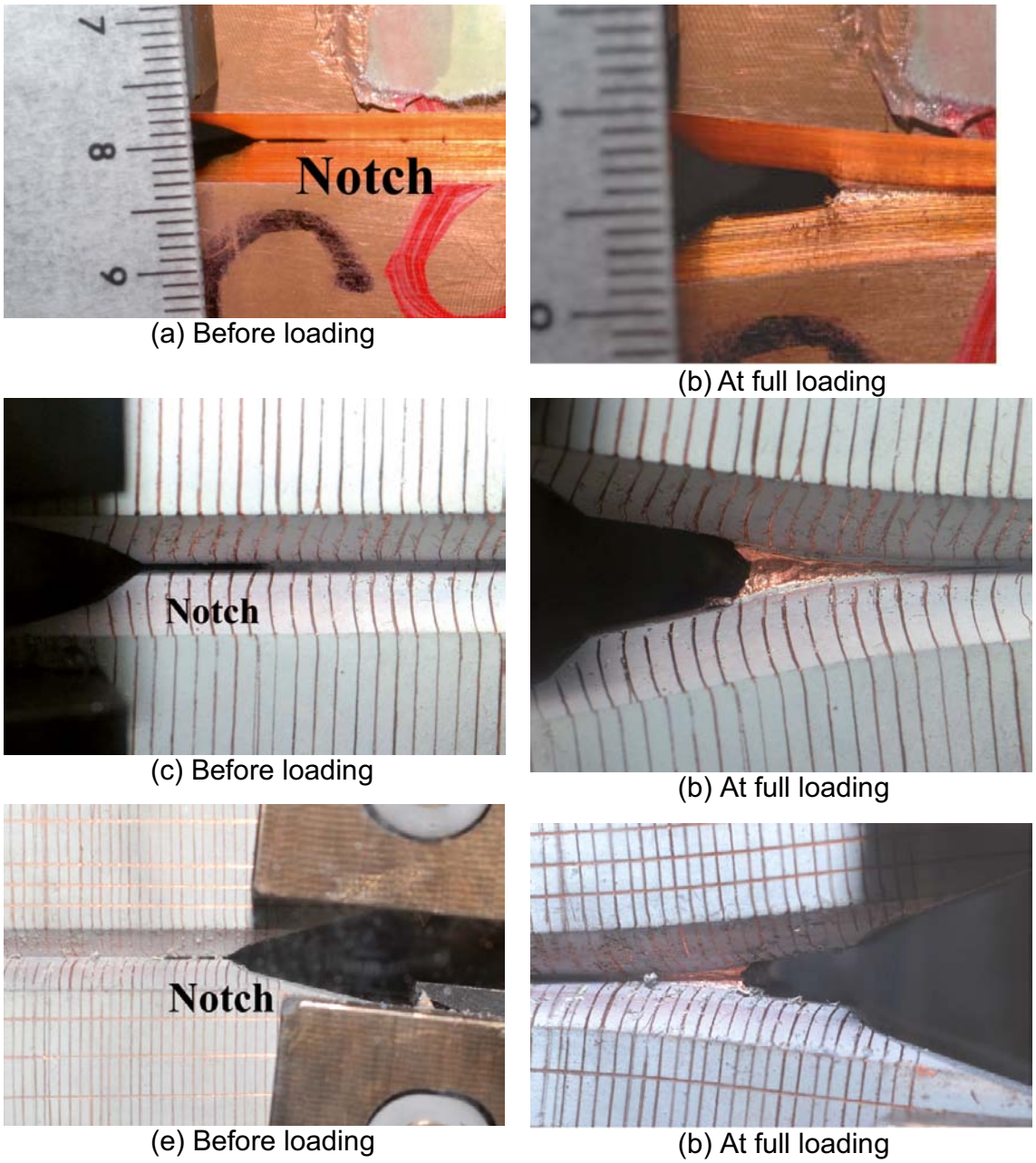

Figure 3-1. *Crack tip opening during uploading. (a) and (b) Specimen CCG22 tested at 22°C and an initial reference stress of 135 MPa. (c) and (d) Specimen CCG75A tested at 75°C and an initial reference stress of 165 MPa. (e) and (f) Specimen CCG75R tested at 75°C and an initial reference stress of 140 MPa.*

Load line displacement (LLD) as a function of time is shown in Figure 3-2 for the CCG tests at 175 and 215°C. Figure 3-2 includes also the normalised potential drop recordings (V/V_0, where V_0 is the initial voltage at time t=0 and V the output voltage at time t) for the test at 175°C. It is seen that LLD increases apparently immediately after full loading. Increment of LLD slows down gradually before LLD increases constantly and LLD rate reaches its minimum value. At the end of the test, increment of LLD accelerates, leading to final failure. At the nearly same reference stress, higher temperature gives a higher LLD rate in the constant increasing region, resulting in a reduced failure time. The constant (minimum) LLD rate is 19.25 µm/h at 215°C and 2.25 µm/h at 175°C, respectively, see Table 3-2. Note that these constant LLD rates are obtained on work hardened copper due to large crack tip opening under uploading.

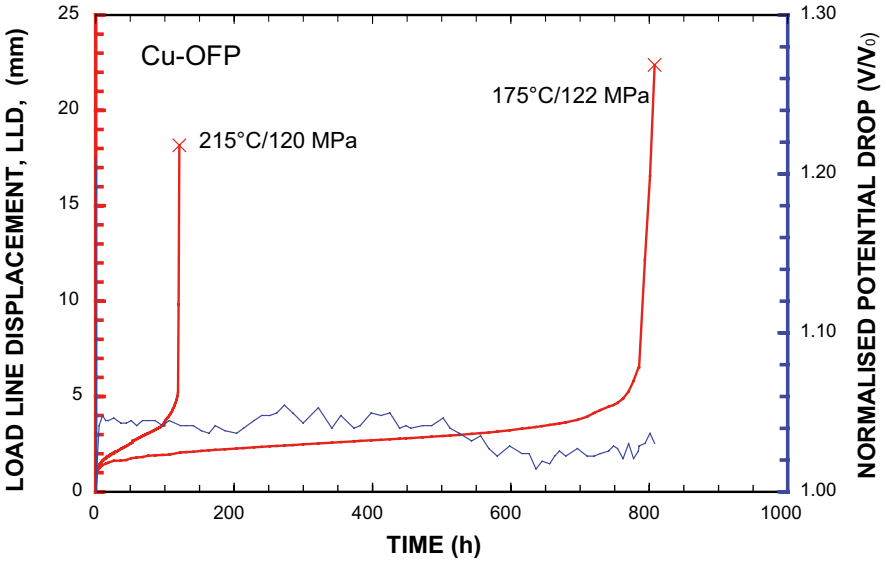

Figure 3-2. Load line displacement (red lines, 175 and 215°C) and normalised potential drop (blue line 175ºC) as a function of time for CCG test.

Table 3-2. CCG testing results.

Specimen	Temperature, T, (°C)	Reference stress, σ_{ref}, (MPa)	Time to rupture, $t_{R,CCG}$ (h)	Minimum load line displacement rate, LLD_{min}, (µm/h)
CCG215	215	120	121	19.25
CCG175	175	122	812	2.25
CCG75A	75	165	Interrupt. at 8925 h	0.0491
CCG75R	75	140–165	Interrupt. at 4778 h	0.079 (at 150 MPa)
CCG22	22	135–205	Interrupt. at 13324 h	0.061 (at 143 MPa)

Actually, the shape of LLD in terms of time is analogue to that of creep curve. There are primary, secondary and tertiary regions. Increase of LLD with time indicates that creep plays a key role in crack tip opening, and eventually advancing. If no creep occurs, LLD does not change, in other words, the slope of LLD would be zero.

The LLD accumulation indicates that there is a long incubation period for the both tests, in which no apparent crack growth could be observed. As soon as the crack started to grow, it accelerated quickly to approach rupture.

It is also seen from Figure 3-2 that the normalised potential drop recording (V/V_0) for the test at 175°C is almost constant with time. This is obviously due to the high electric conductivity of copper. Usually, V/V_0 increases as soon as cross section area decreases as a result of crack growth. Theoretically, the accumulated crack length Δa can be calculated according to an analytical solution recommended by the standard ASTM E 1457 (ASTM 2000, Johnson 1962)

$$\Delta a = \frac{2W}{\pi}\cos^{-1}\left\{\frac{\cosh(\pi Y_0/2W)}{\cosh\left[\frac{V}{V_0}\cosh^{-1}\left(\frac{\cosh(\pi Y_0/2W)}{\cos(\pi a_0/2W)}\right)\right]}\right\} - a_0 \qquad (3\text{-}2)$$

where a_0 is the initial crack length in mm with respect to the initial voltage V_0 at time t=0, and Y_0 the half distance between the output voltage leads in mm. In the present case, Y_0 is about 12 mm.

Unfortunately, eqn. (3-2) cannot be applied to calculate the crack length, simply because of practically unchanged V/V_0, no matter whether there is crack growth during testing.

Load line displacement (LLD) as a function of time is shown in Figure 3-3 for the CCG tests at 75°C. Figure 3-3 also includes the normalised potential drop recordings, V/V_0, for the test at 165 MPa. The V/V_0 recordings for the incremental test from 140 to 165 MPa are similar to that at 165 MPa. Both tests have been interrupted after 4778 hours and 8925 hours, respectively.

For the specimen CCG75A, LLD has accumulated to 2.45 mm after commencement of test, see Figure 3-3. The LLD rate has a minimum value of 0.049 µm/h, see Table 3-2. Again, this value is obtained on work hardened copper due to large crack tip opening under uploading.

For the specimen CCG75R, the reference stress has been raised from initially 140 to 165 MPa before it is interrupted, see also Figure 3-3. Accumulation of LLD at 140 MPa is 1.26 mm after 695 hours, including once loading bar arm level readjustment. During this period, the crack tip opening and growth are continuously monitored. Because there is no crack growth, the reference stress is raised to 150 MPa. This results in an instantaneous LLD increase of 0.46 mm. The test at 150 MPa runs until 3096 hours. After verification of no crack growth, the reference stress is increased again to 165 MPa. At this time, an instantaneous LLD increase of 1.34 mm is recorded. Since there is no obvious indication of crack growth (see later), the test is interrupted after 4778 hours. The total LLD during CCG test is 5.70 mm, see also Table 3-1. Due to short term test at each reference stress, the minimum LLD rate might not have been approached. An estimation of the minimum LLD rate at 150 MPa, which has a relative long test duration, is 0.079 µm/h, see Table 3-2.

The normalised potential drop recording (V/V_0) for the specimen CCG75A is to a large extent unchanged, although it fluctuates and disturbances from electrical supply system causing abrupt drop and jump are visible.

Load line displacement (LLD) and normalised potential drop recording (V/V_0) as a function of time are shown in Figure 3-4 for the CCG test at 22°C, the specimen CCG22. The initial reference stress is set to be 135.5 MPa. After one day, the reference stress is raised to 143.3 MPa since it is believed that 135.5 MPa was to low. The test at 143.3 MPa continues until 4560 hours. During this period, the crack tip opening and growth are continuously observed. Like the incremental test at 75°C, the reference stress has been raised several times to the final stress 205 MPa, including once loading bar arm level readjustment. Since there is no obvious indication of crack growth (see later), the test is interrupted after 13324 hours. The total LLD during CCG test is 15.10 mm, see also Table 3-1. Relative long test is only obtained at 143.3 MPa. The minimum LLD rate at this reference stress is estimated to be 0.061 µm/h, see Table 3-2. Again, this value is obtained on work hardened copper due to large crack tip opening under uploading.

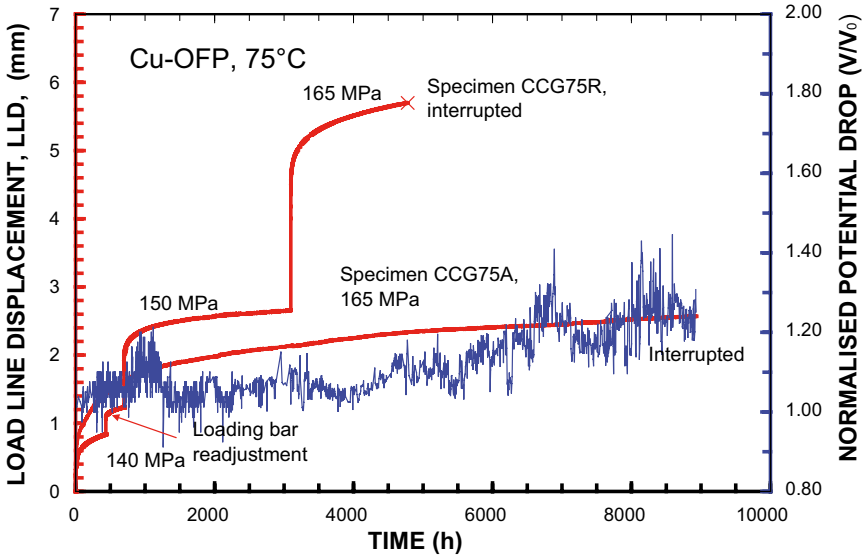

Figure 3-3. *Load line displacement (red lines) and normalised potential drop for the test at 165 MPa (blue line) as a function of time for the CCG tests at 75°C.*

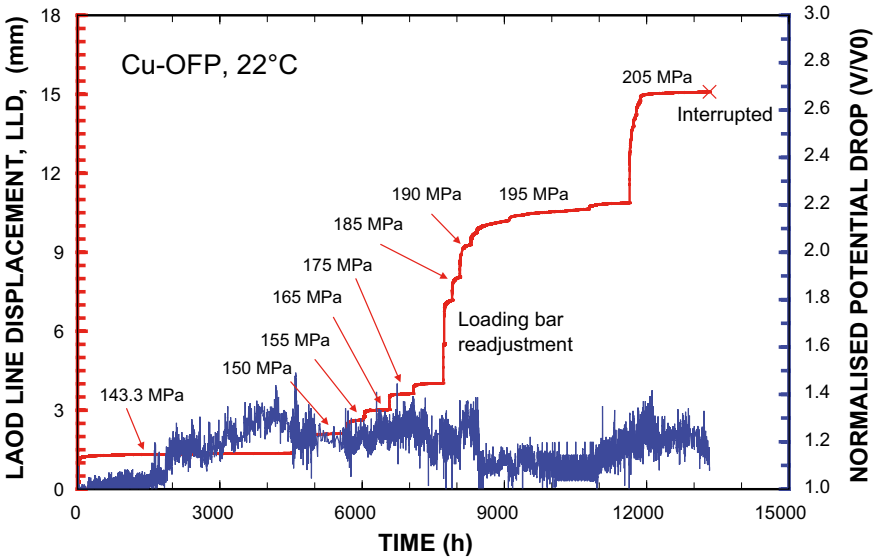

Figure 3-4. *Load line displacement (red line) and normalised potential drop (blue line) as a function of time for the CCG tests at 22°C.*

The normalised potential drop recording (V/V_0) for the test at 22°C falls within a narrow band between 1.1 to 1.3, see Figure 3-4.

Time to rupture under CCG, $t_{R,CCG}$, and time to rupture under uniaxial creep, $t_{R,Uni}$, are given in Table 3-3. The values of $t_{R,Uni}$ are taken from various references. It is clear that, at 215°C, $t_{R,CCG,}$ is shorter than $t_{R,Uni}$ by a factor up to 65. At 175°C, this factor becomes even larger, *e.g.* several orders of magnitude, see Figure 3-5. Time to rupture under both uniaxial and CCG tests at 22 and 75°C are not available.

Table 3-3. Comparison of CCG and uniaxial testing results.

CCG test		Uniaxial plain creep test		$t_{R,CCG}$ /	Ref.
T/σ_{ref} (°C/MPa)	$t_{R,CCG}$ (h)	T/stress (°C/MPa)	$t_{R,Uni}$ (h)	$t_{R,Uni}$	
215/120	121	215/120	2133~7848	18~65	1, 2
175/122	812	175/130	>20763	>25.6	3
75/165	Interrupt. at 8925 h	75/170	>9585		4
75/140–165	Interrupt. at 4778 h	75/170	>9585		4
22/135–205	Interrupt. at 13324 h				

T is temperature, $t_{R,CCG}$ and $t_{R,Uni}$ are time to rupture by CCG and by uniaxial creep, respectively.

[1)] Seitisleam and Henderson 1997

[2)] Henderson and Werme 1996

[3)] Andersson et al. 2005

[4)] Andersson et al. 2007

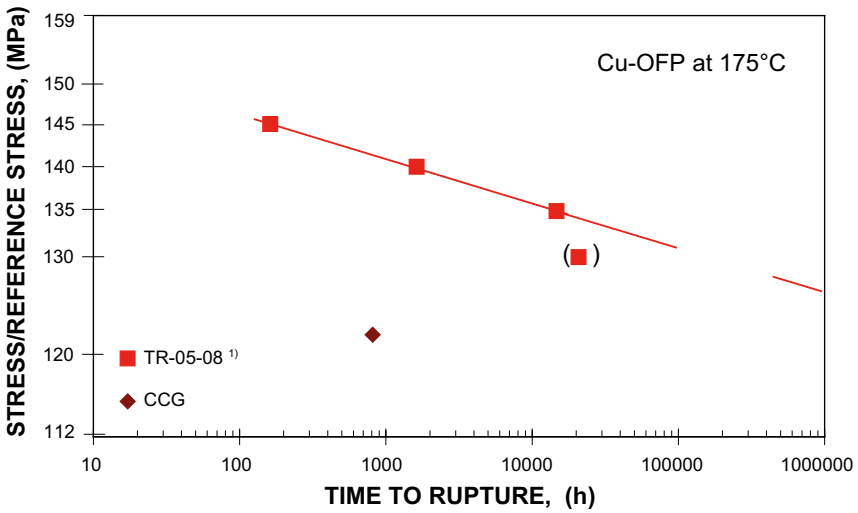

1) Andersson et al. 2005

Figure 3-5. *Stress (uniaxial) and reference stress (CCG) as a function of time to rupture for Cu-OFP at 175°C.*

3.2 Observation of crack tip opening and growth at 22 and 75°C

Crack tip opening and growth after full loading has been continuously observed for the tests at 22 and 75°C. Selected images of crack tip for the test at 22°C, the specimen CCG22, are given in Figure 3-6. The images are regularly taken, once a week. After full loading, crack tip continues to blunt and there seems to be a crack branching and growth (about 0.5 mm), see Figures 3-6a and 3-6b. With increasing time and reference stress, material around the crack tip deforms more, the crack opens larger, and more crack branching is observed, see Figure 3-6c. Further increase in time and reference stress leads to actually crack tip sharpening, more branching, tearing, see Figures 3-6d and 3-6e. From the front of the crack, elongated and heavily deformed grains can be seen, see Figures 3-6f and 3-6h. In addition, material in front of the crack 'shrinks' towards inside. At interruption, material seems to have separated at outer surface, see Figures 3-6g and 3-6f.

Selected images of crack tip for the specimen CCG75R are given in Figure 3-7. Like the test at 22°C, the images are regularly taken. After full loading, crack tip blunts and there seems a crack branching, see Fig 3-7a. With increasing time to 597 hours, there is no any apparent change in crack tip, see Figures 3-7a and 3-7b. The reference stress is then raised to 150 MPa and this stress is kept until 3096 hours before it is increased to 165 MPa. During this period, material around the crack tip deforms more, the crack opens further, and more crack branching seems to have occurred, see Figures 3-7c–3-7e. At interruption, crack tip sharpening and more opening takes place, see Figure 3-7f. With the help of measuring net, it is seen there is no crack growth.

Selected images of crack tip for the specimen CCG75A are given in Figure 3-8. After full loading, crack tip blunts and there is crack branching on the surface, see Fig 3-8a. After 546 hours, this crack branching has changed its appearance, see Figure 3-8b. With increasing time, there seems no obvious change in crack tip, although the crack continues to open more, see Figures 3-8c–3-8f. With the help of measuring net, it is easy to say that the crack has not started to grow.

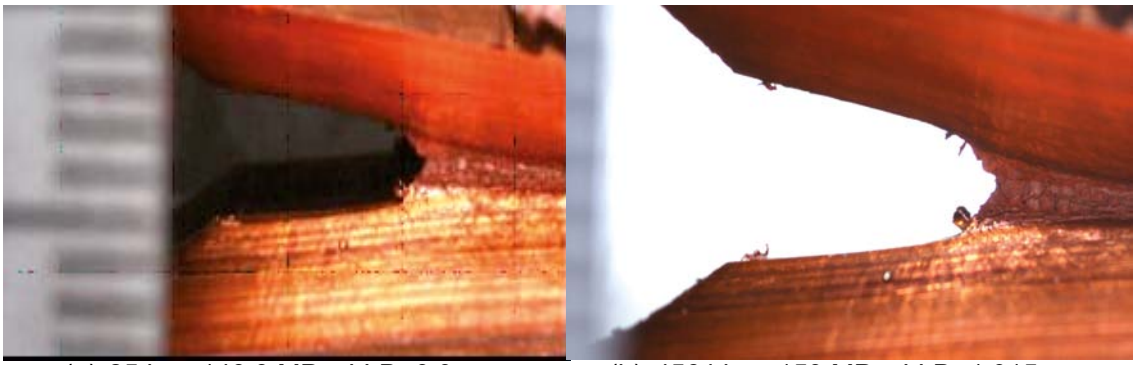

(a) 25 hrs, 143.3 MPa, LLD=0.9 mm (b) 4564 hrs, 150 MPa, LLD=1.915 mm

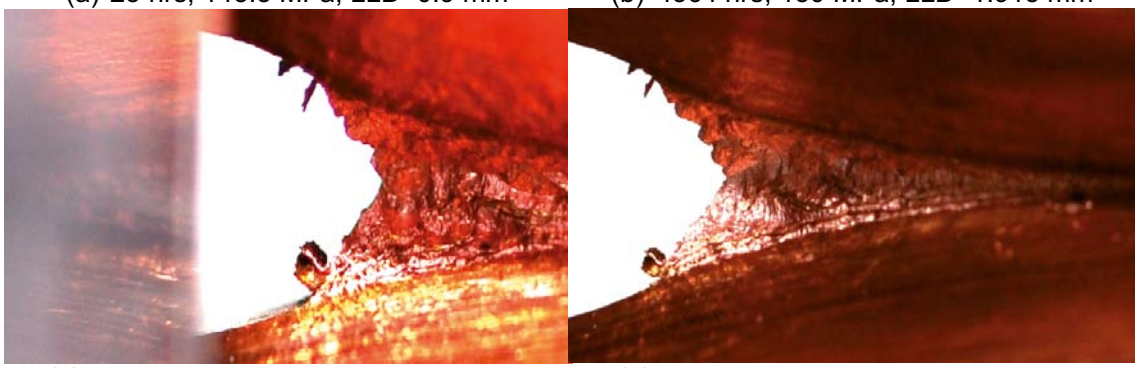

(c) 6576 hrs, 175 MPa, LLD=3.463 mm (d) 7897 hrs, 190 MPa, LLD=7.22 mm

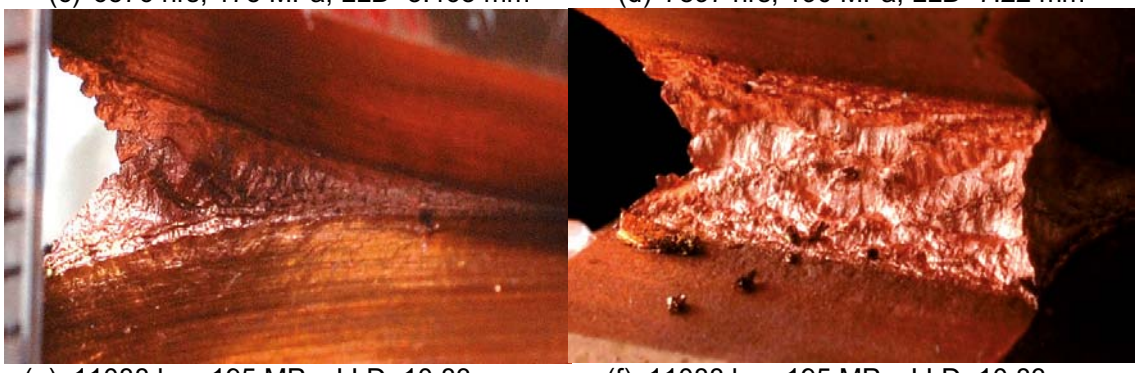

(e) 11088 hrs, 195 MPa, LLD=10.83 mm (f) 11088 hrs, 195 MPa, LLD=10.83 mm

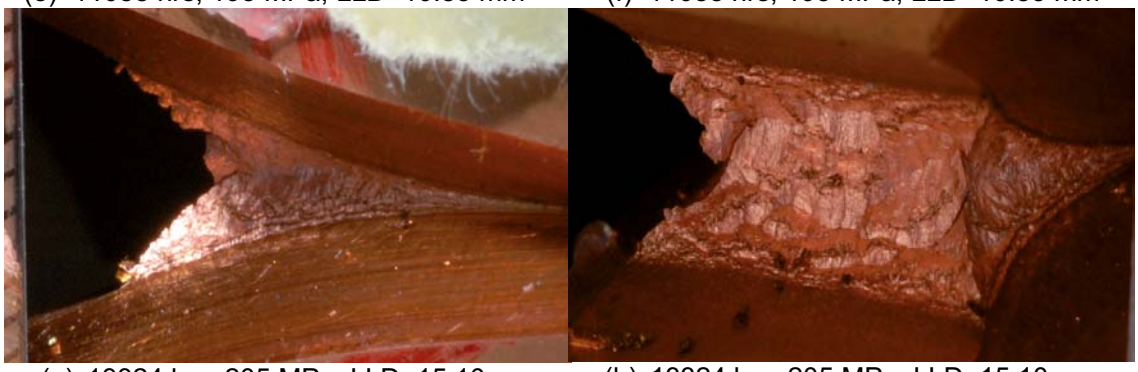

(g) 13324 hrs, 205 MPa, LLD=15.10 mm (h) 13324 hrs, 205 MPa, LLD=15.10 mm

Figure 3-6. *Crack tip opening under CCG test at 22°C, specimen CCG22. All the images are taken from the side of the CT specimen, except (f) and (h) are from the front. Test duration, reference stress and LLD are given for each corresponding image.*

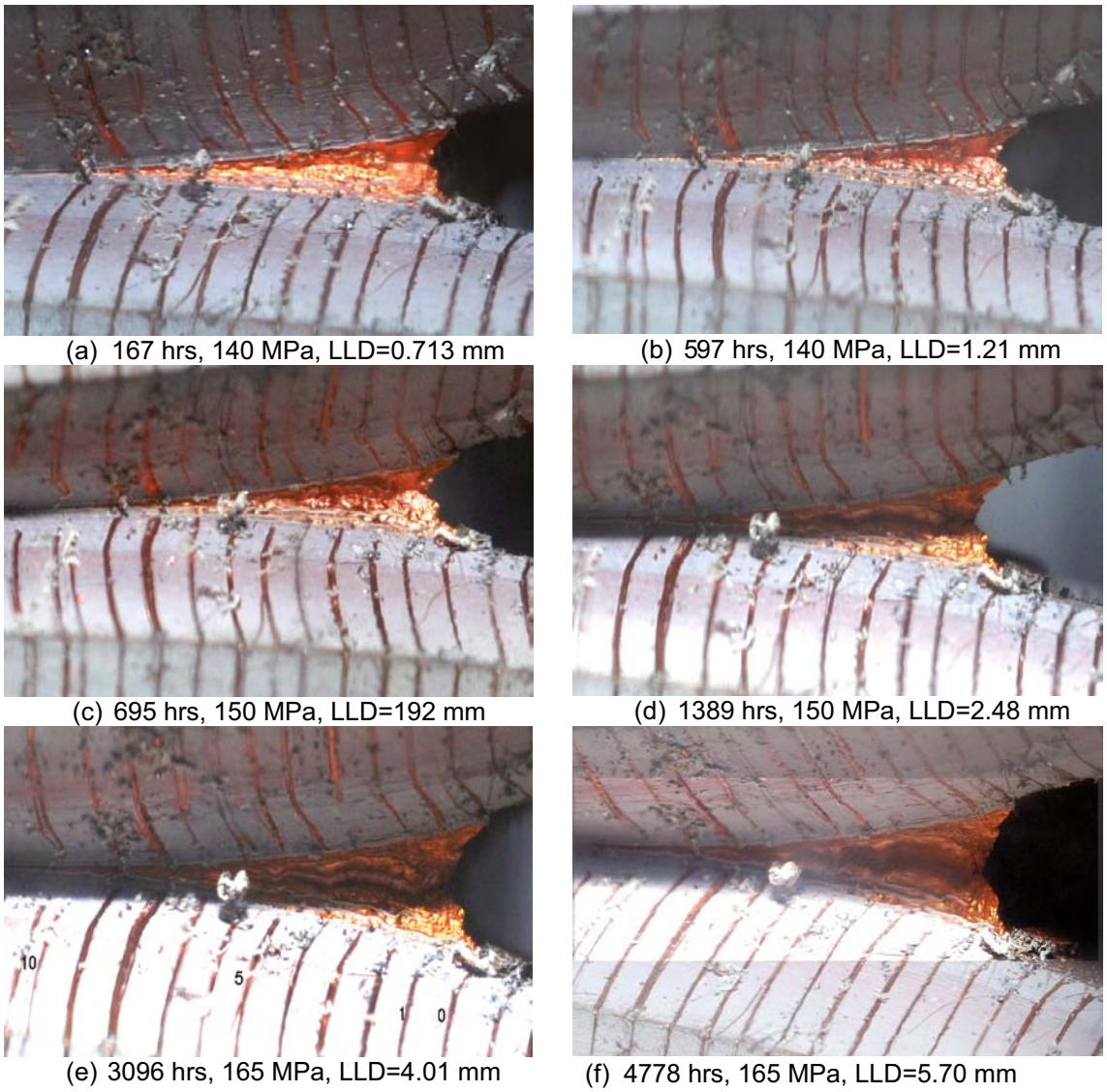

Figure 3-7. *Crack tip opening under CCG test at 75°C for specimen CCG75R. All the images are taken from the side of the CT specimen. Test duration, reference stress and LLD are given for each corresponding image.*

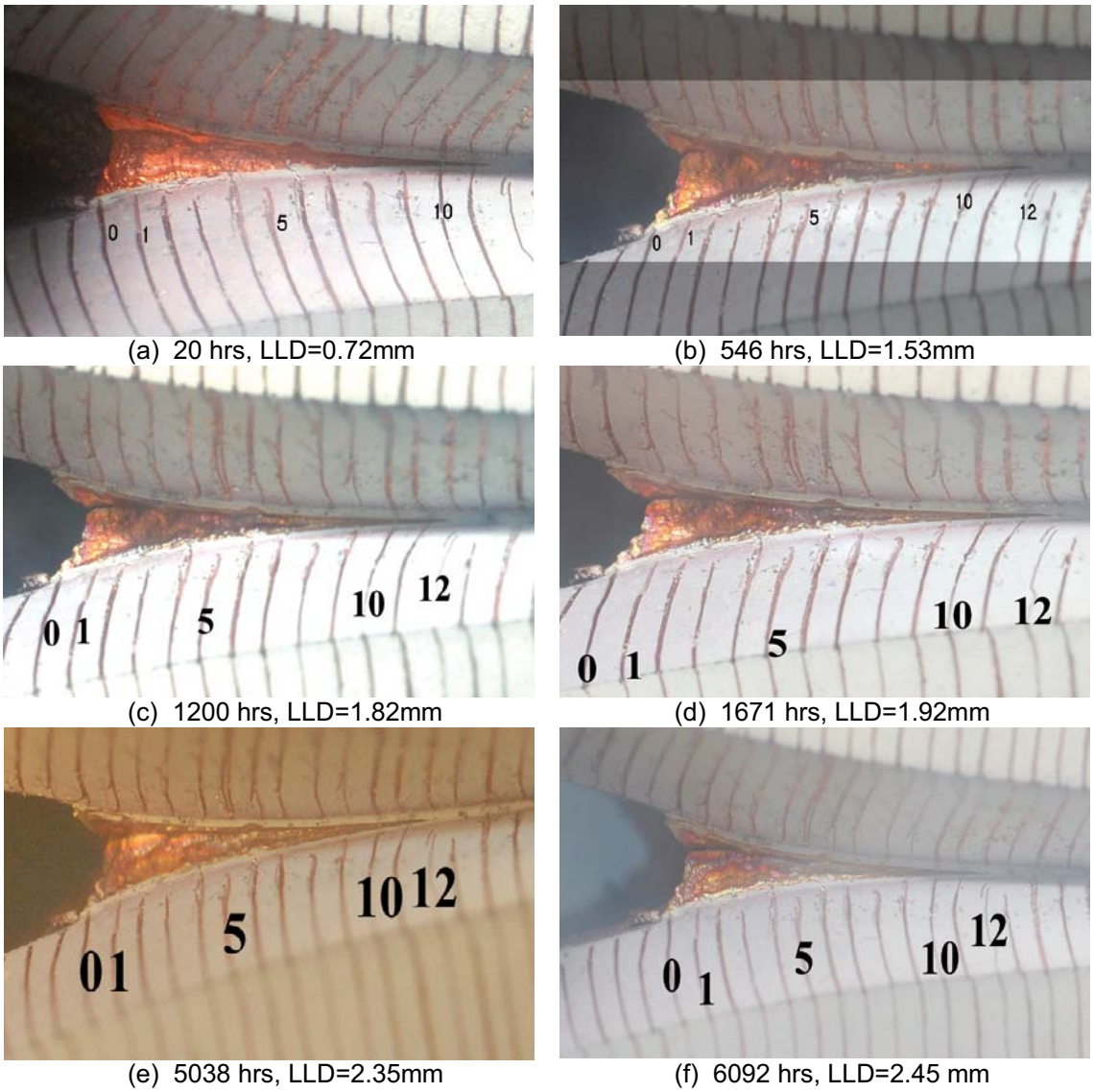

(a) 20 hrs, LLD=0.72mm (b) 546 hrs, LLD=1.53mm

(c) 1200 hrs, LLD=1.82mm (d) 1671 hrs, LLD=1.92mm

(e) 5038 hrs, LLD=2.35mm (f) 6092 hrs, LLD=2.45 mm

Figure 3-8. *Crack tip opening under CCG test at 75°C for specimen CCG75A. All the images are taken from the side of the CT specimen. Test duration and LLD are given for each corresponding image.*

3.3 Post test metallography

3.3.1 Ruptured CCG tests at 175 and 215°C

After rupture, length of crack growth is determined by observing fracture surface where the crack growth zone is heavily oxidised, see Figure 3-9. For both tests, the crack has grown approximately 10 mm before rapid separation.

Side view of CT specimens after failure for tests at 175 and 215°C is given in Figure 3-10. Since the weight has landed on the floor, the CT specimens are not fully separated. Indeed, Figure 3-10 shows the crack growth.

Figure 3-9. *LOM image showing fracture surface for CCG215, test at 215°C.*

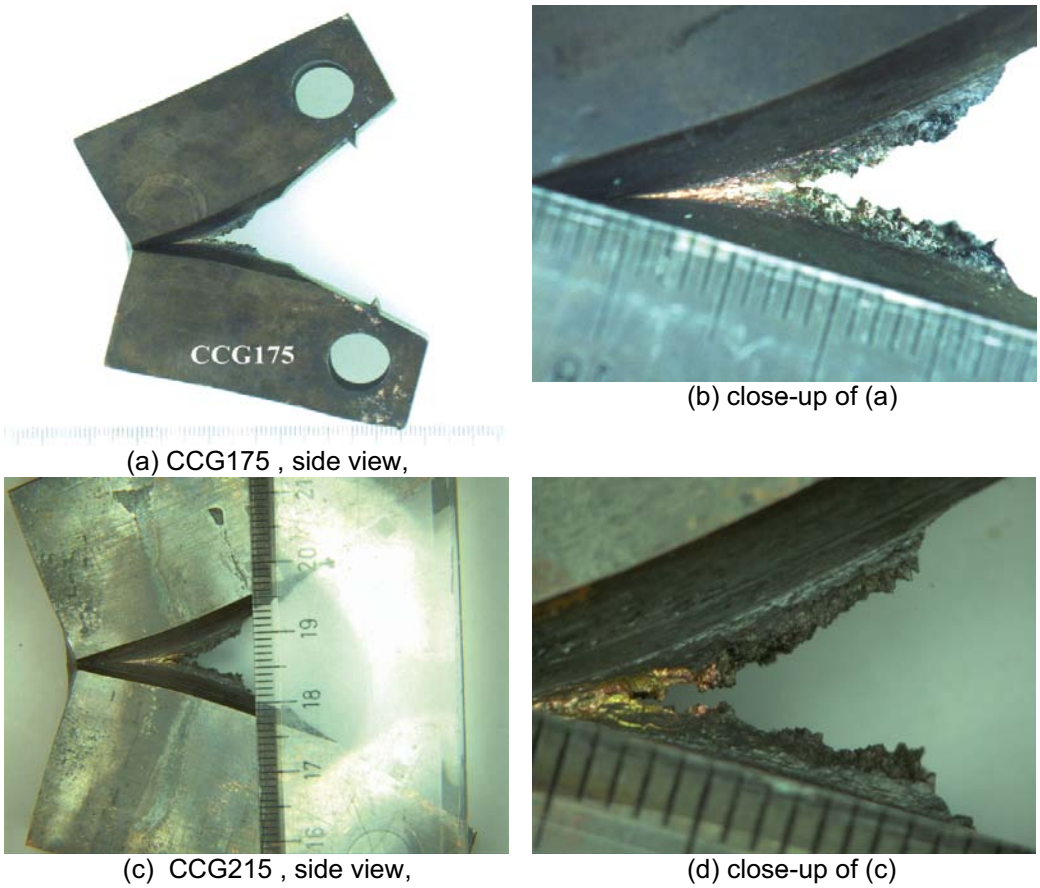

(a) CCG175 , side view,

(b) close-up of (a)

(c) CCG215 , side view,

(d) close-up of (c)

Figure 3-10. *LOM images showing CT specimens after failure. (a) and (b) 175°C. (c) and (d) 215°C*

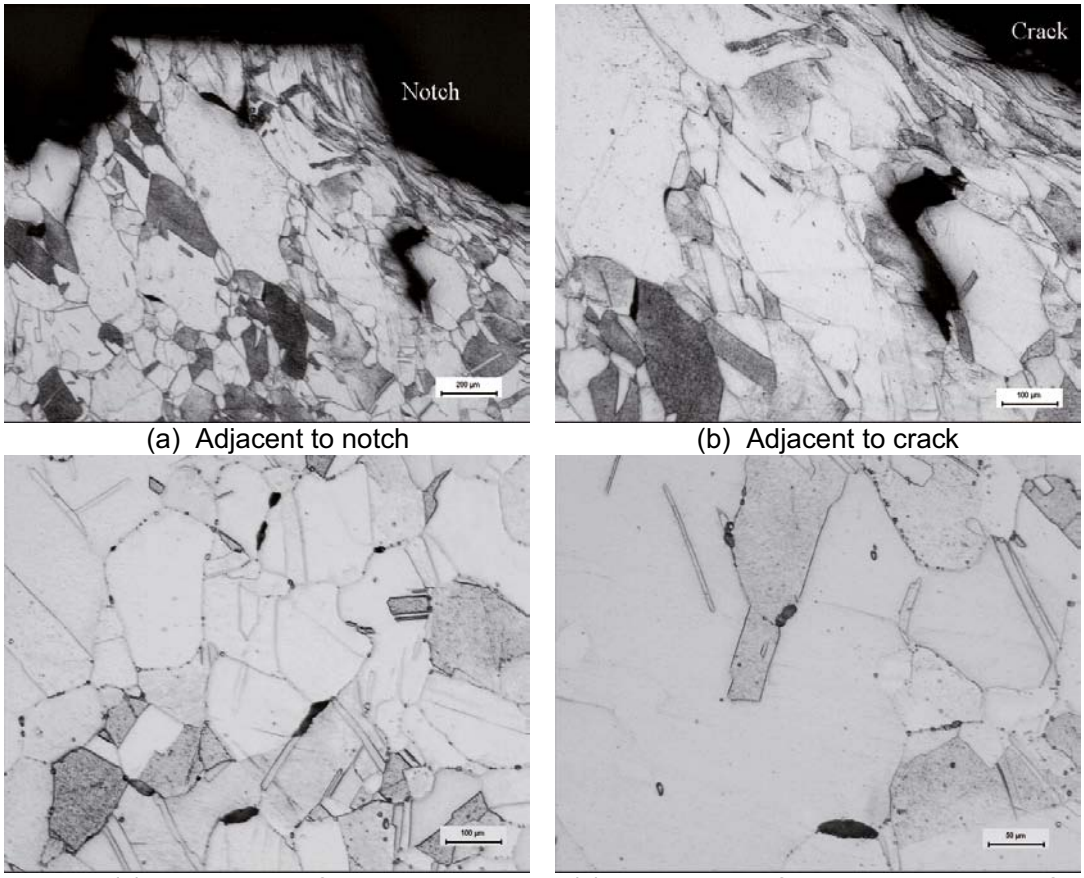

Figure 3-11. *LOM images after failure showing creep cavities and microcracks around notch and crack for specimen CCG175, tested at 175°C. Crack grows from the right to the left.*

Strongly elongated and deformed grains adjacent to notch are observed on the failed specimen CCG175, tested at 175°C, see Figures 3-11a and 3-11b. Extensive creep damage in terms of cavities and microcracks are visible several mm from the crack, see Figures 3-11c and 3-11d. Creep damage appears on the grain boundary, preferably on the mixed grain boundaries where small and large grains meet, see Figures 3-11a, 3-11b and 3-11d.

The results of post test metallography for the failed specimen CCG215, tested at 215°C, are similar to those for CCG175, see Figure 3-12.

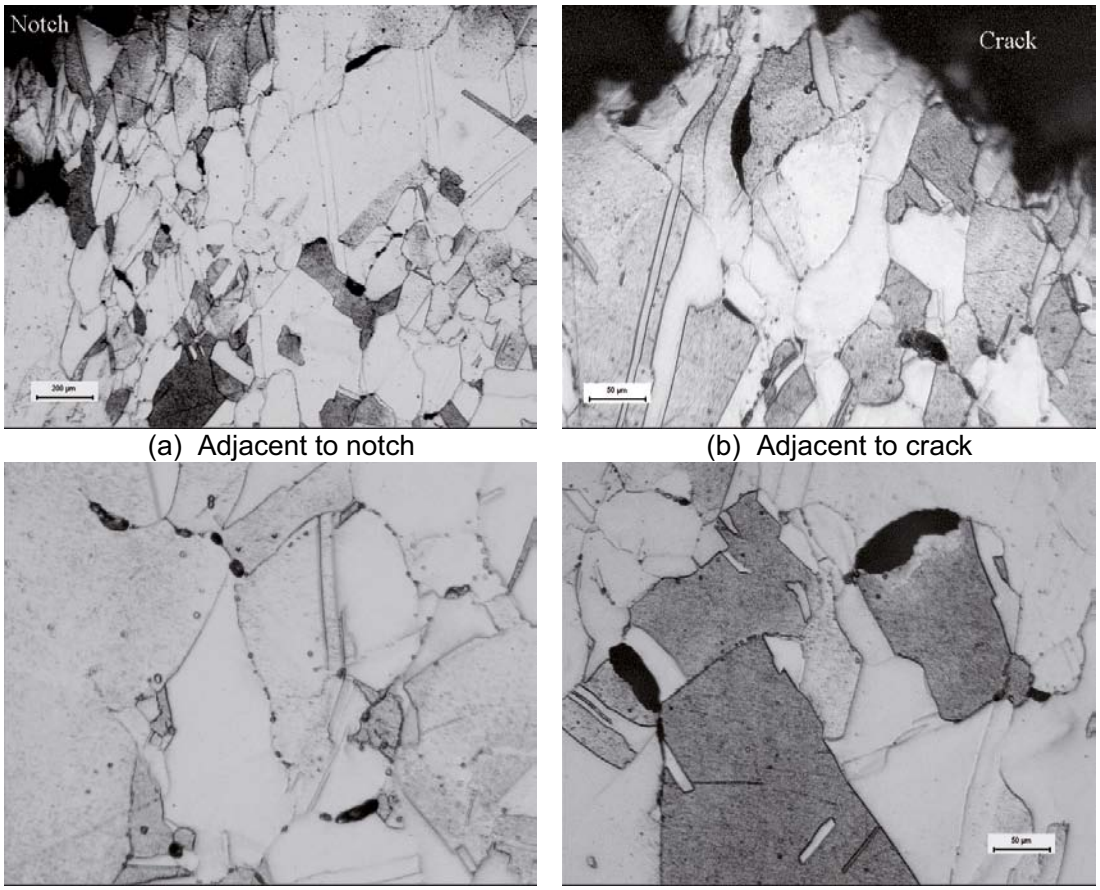

Figure 3-12. *LOM images after failure showing creep cavities and microcracks around notch and crack for specimen CCG215, tested at 215°C. Crack grows from the left to the right.*

3.3.2 Interrupted CCG tests at 22 and 75°C

The CT specimens after interruption have been investigated before sectioning along the crack plane, see Figure 3-13. It is seen that both specimens are heavily deformed. This is more pronounced for CCG22. From the side view, see Figure 3-13c, it clear that both specimens are bent. The upper and lower surfaces are no longer straight.

Observations of the crack appearance from side and from front are shown in Figure 3-14 for CCG22, interrupted test at 22°C. From both sides, it is seen that surface cracks have initiated, see Figures 3-14a–3-14c. Viewing from front shows that the surface cracks propagate about 45° to the load direction towards inside, see Figures 3-14d and 3-14e. In the middle of the crack, propagation of crack is seen at several sites, indicated by arrows, see Figure 3-14f.

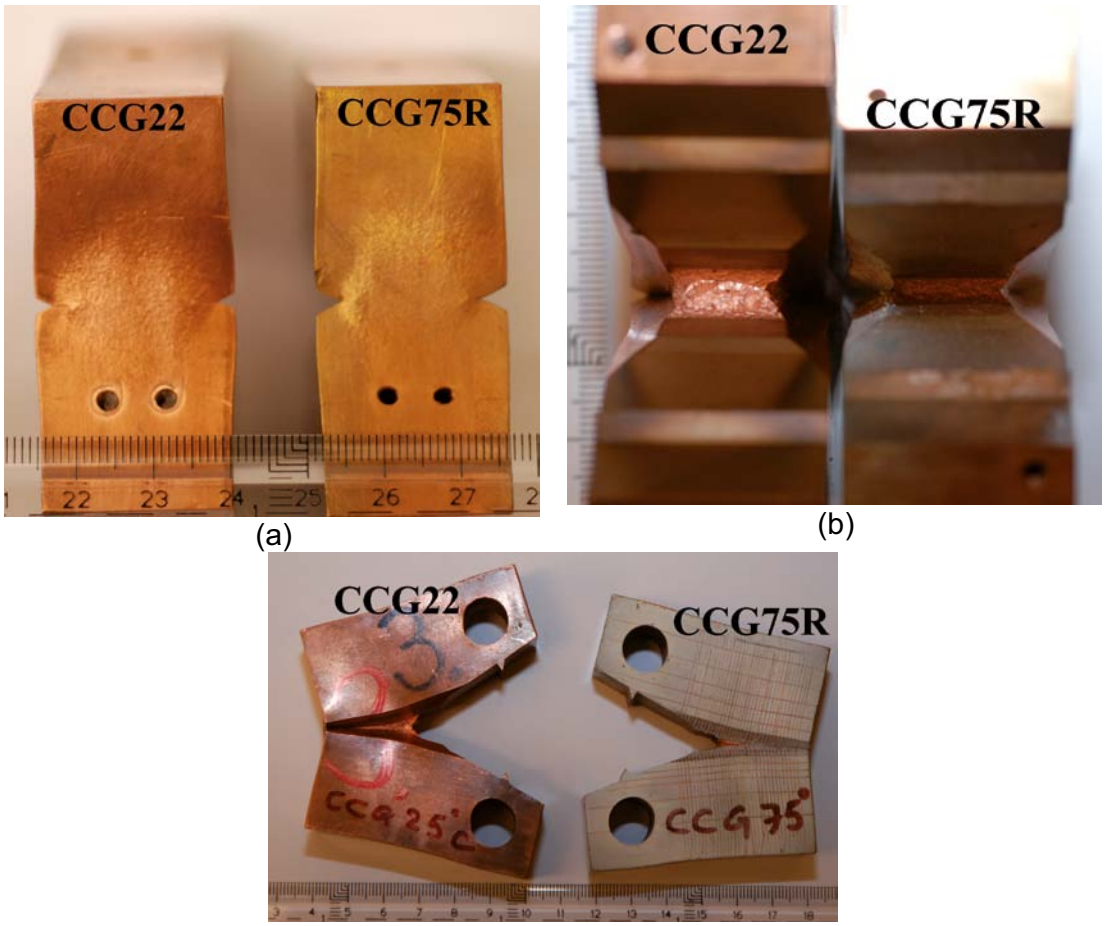

Figure 3-13. *Interrupted CT specimens CCG22 and CCG75R. Different views from (a) back surface. (b) front and (c) side.*

Similar findings are also found for CCG75R, interrupted test at 75°C. Surface cracks have initiated and propagated about 45° to the load direction towards inside. However, there is no crack appearance like that exhibited in Figure 3-14, implying no crack growth.

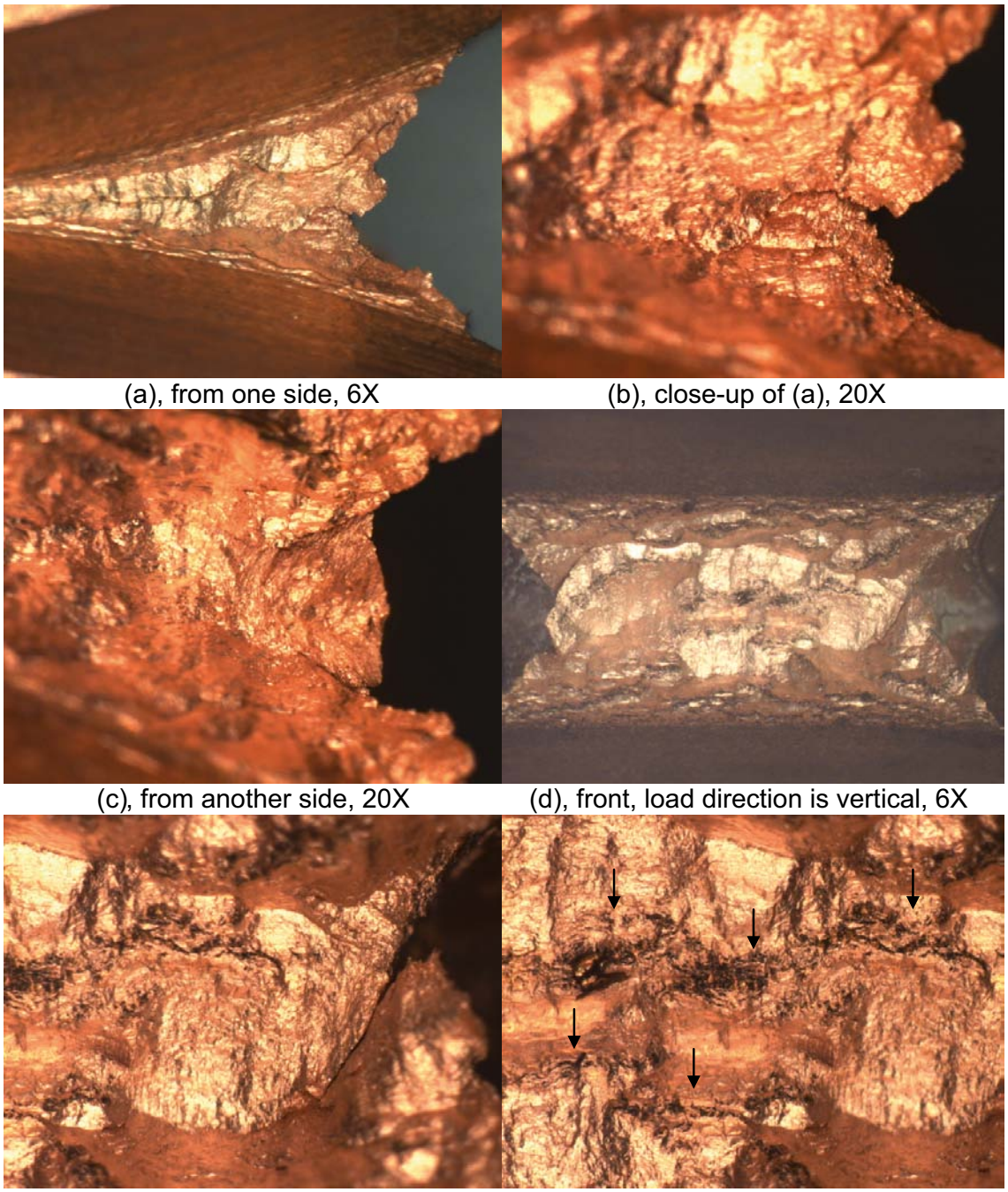

Figure 3-14. *LOM images showing crack appearance from side and front for CCG22, interrupted test at 22°C.*

After sectioning in the middle of CT specimen, hardness very close to the crack tip, distance between crack tip and back surface (corresponding to W-a in Table 2-1), and crack tip opening are measured for the specimens CCG22 and CCG75R, see Table 3-4, and Figure 3-15. In Table 3-4 the corresponding values prior to testing are given for comparison.

Table 3-4. Various measurements at interruption for CT specimens CCG22 and CCG75R.

	Hardness		W-a (mm)		Crack tip opening (mm)	
	Before test	At interrupt.	Before test	At interrupt.	Before test (notch diameter)	At interrupt.
CCG22	54	129.6	25.07	24.306	0.30	3.312
CCG75R	54	112.4	25.049	25.025	0.30	1.437

Hardness adjacent to crack tip for both specimens has more than doubled as a consequence of work hardening, or heavy deformation. This can be also verified by strong crack tip opening, c.f. Figure 3-15. If the notch diameter before testing of 0.3 mm is assumed, the true strain at the crack tip is estimated to 10 and 4 for CCG22 and CCG75R, respectively. This is an extremely large deformation. Considering the (W-a) values before and after testing, it seems the crack is still at the incubation stage. This is more obvious for CCG75R, for instance, only 0.024 mm in difference. For CCG22, this value is 0.71 mm. There is an apparent crack branching and propagation for CCG22, see Figure 3-14a, which agrees with observation shown in Figure 3-14f.

Metallographic examination near crack tip for CCG22, interrupted test at 22°C, shows strongly elongated and deformed grains, see Figures 3-16a and 3-16b. Microcracks are found and they tend to propagate intergranularly, see Figure 3-16b. Near the crack tip, there are creep cavities and microcracks, see Figures 3-16c and 3-16d. This is verified by FEG-SEM as well, see Figures 3-16e and 3-16f.

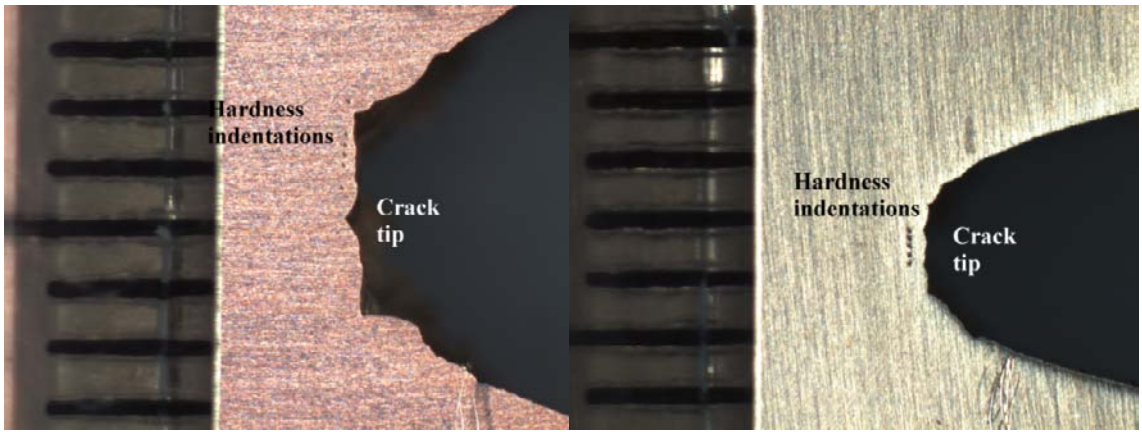

Figure 3-15. *Hardness close to crack tip, and crack tip opening in the middle section at interruption.*

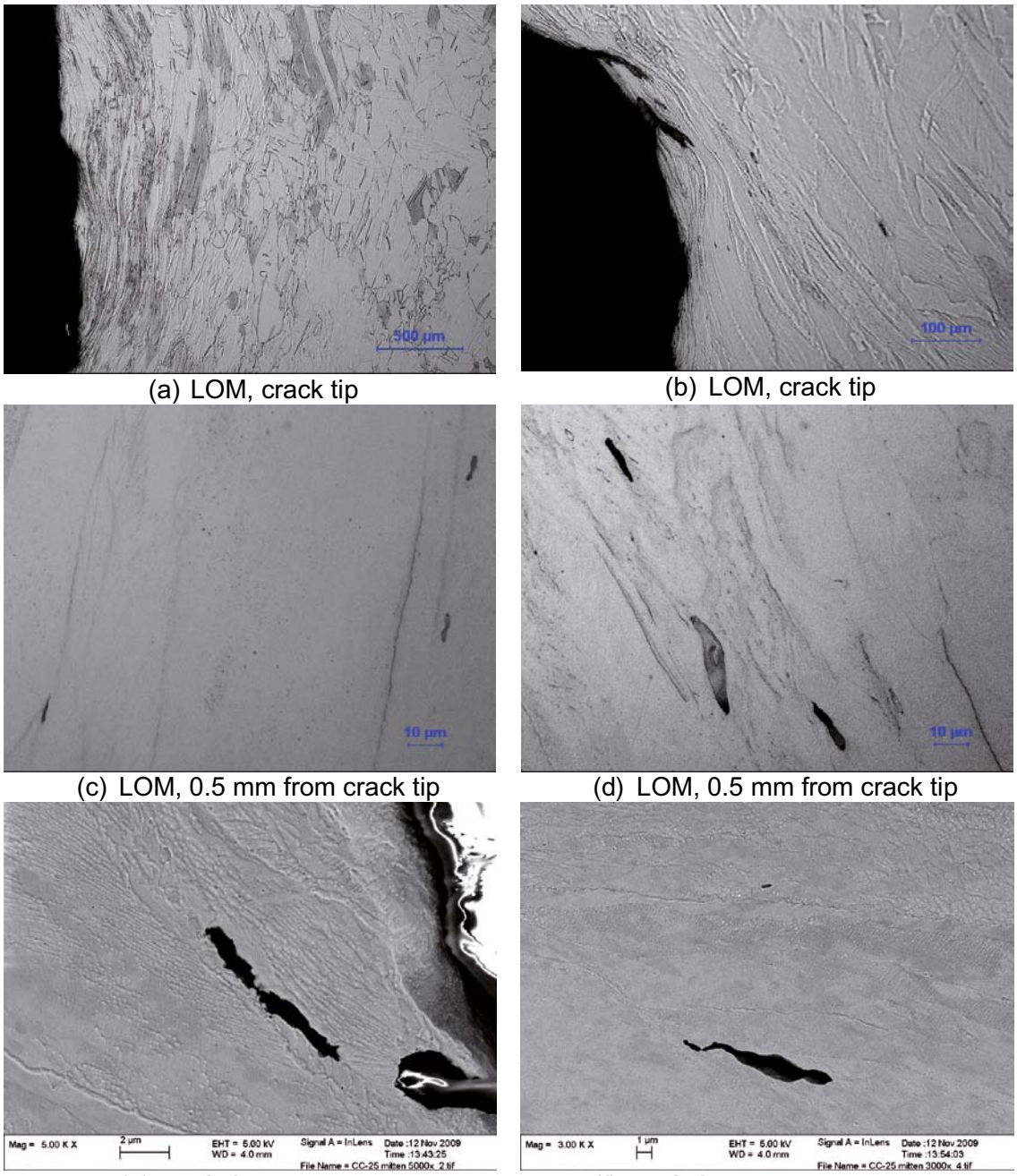

(a) LOM, crack tip (b) LOM, crack tip

(c) LOM, 0.5 mm from crack tip (d) LOM, 0.5 mm from crack tip

(e) FEG-SEM, crack tip (f) FEG-SEM, close to crack tip

Figure 3-16. *Metallographic examination for CCG22, interrupted test at 22°C.*

Metallographic examinations for CCG75R, interrupted test at 75°C, show similar results to those for CCG22. Strongly elongated and deformed grains as well as microcracks are visible, see Figure 3-17a. Near the crack tip, there are creep cavities and microcracks, see Figs. 3-17b and 3-17c.

(a) LOM, crack tip

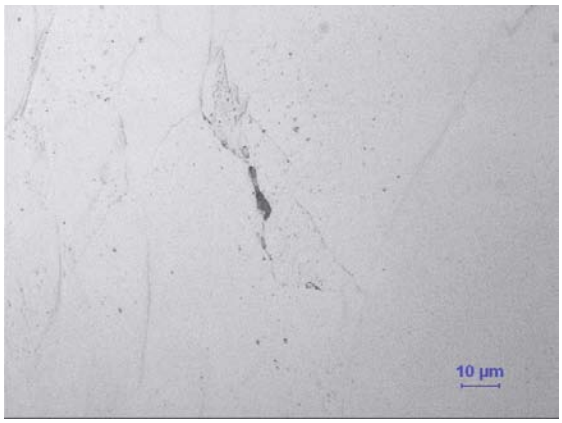

(b) LOM, crack tip

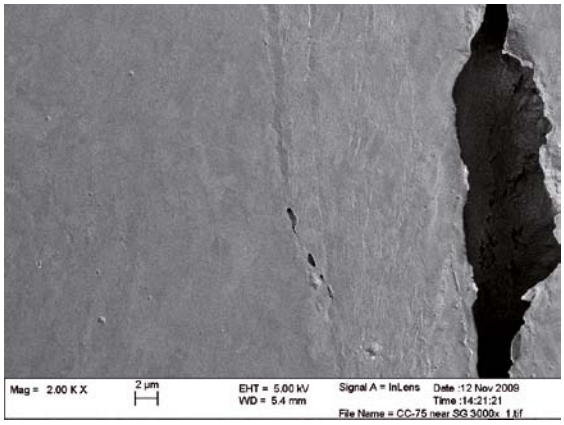

(c) FEG-SEM, close to crack tip

Figure 3-17. *Metallographic examination for CCG75R, interrupted test at 75°C.*

4 Modelling creep crack growth

4.1 Description of creep damage

Creep damage can take many forms such as creep cavity formation, particle coarsening, and substructure growth. The most important one of these is cavitation, which controls the final creep rupture. It has been demonstrated that nucleation and growth of creep cavities increases with creep strain (Sandström and Wu 2007, Wu and Sandström 1996). Consequently, it is natural to try to relate the generation of creep damage directly to the creep strain. The damage development $\dot{\omega}$ can then be formulated as

$$\dot{\boldsymbol{\omega}} = D\dot{\boldsymbol{\varepsilon}}_{\mathrm{c}}(T,\boldsymbol{\sigma})f_{\mathrm{multi}} \tag{4-1}$$

where $\dot{\boldsymbol{\varepsilon}}_{\mathrm{c}}$ is the creep strain rate tensor, T the temperature, σ the effective stress, f_{multi} a factor that takes the effect of multiaxiality on the damage into account, and D a constant. The creep damage has the same dimension as the strain rate, i.e. 1/s. f_{multi} is often expressed in one the following alternative forms, see for example Lin et al. (2005)

$$f_{\mathrm{multi}} = \left(\frac{\sigma_1}{\sigma_{\mathrm{e}}}\right)^{\gamma n} \tag{4-2a}$$

$$f_{\mathrm{multi}} = \left(\frac{\alpha\sigma_1 + (1-\alpha)\sigma_{\mathrm{e}}}{\sigma_{\mathrm{e}}}\right)^{n} \tag{4-2b}$$

where σ_1 is the largest principal stress, σ_e the effective stress, n the Norton exponent, and α and γ constants. In the uniaxial case, $\sigma_1 = \sigma_e$ and the expressions in eq. (4-2) are equal to unity. For OFP copper a fundamental model has been formulated for the uniaxial creep strain rate (Sandström and Andersson 2008)

$$\dot{\varepsilon}_{\mathrm{OFP\,stat}} = \frac{2bc_L}{m}\frac{D_{s0}b\tau_L}{k_BT}\left(\frac{\sigma}{\alpha mGb}\right)^3 e^{\frac{\sigma b^3}{k_BT}} e^{-\frac{Q}{RT}\left[1-\left(\frac{\sigma}{\sigma_{i\max}}\right)^2\right]} / f_P \tag{4-3}$$

Eq. (4-3) gives the stress dependence of the stationary creep rate. The interpretation and the values of the parameters in (4-3) can be found in Sandström and Andersson (2008). All the parameter values are fixed and are not used for fitting to data. Using Odqvist's relation, eq. (4-3) can directly be transferred to the multiaxial case (Sandström and Andersson 2008).

$$\dot{\boldsymbol{\varepsilon}}(T,\boldsymbol{\sigma}) = \frac{3}{2}\dot{\varepsilon}_{\mathrm{OFP\,stat}}(\sigma_{\mathrm{e}})\frac{\boldsymbol{\sigma}'}{\sigma_{\mathrm{e}}} \tag{4-4}$$

$\boldsymbol{\sigma}'$ is the stress deviator tensor. Its component perpendicular to the crack plane σ'_z is of most direct interest in this investigation. As is customary, the damage parameter is assumed to take the value unity at failure. This implies that the constant D is related to the creep ductility A_{c}.

$$D = \frac{1}{A_{\mathrm{c}}} \tag{4-5}$$

The creep ductility for Cu-OFP in the temperature interval 75 to 300ºC has been found to be in the range 30 to 50% (Andersson and Sandström 2009). In (8) a value of $A_c = 0.4$ has been assumed. For a fixed temperature and stress, $\dot{\varepsilon}_{\mathrm{c}}$ is constant and the rupture t_{R} can be obtained directly

$$t_{\mathrm{R}} = \frac{A_{\mathrm{c}}}{\dot{\varepsilon}_{\mathrm{cz}}(T,\sigma_{\mathrm{e}})f_{\mathrm{multi}}} \tag{4-6}$$

In Figure 4-1, eq. (4-6) is compared to uniaxial creep rupture data for Cu-OFP.

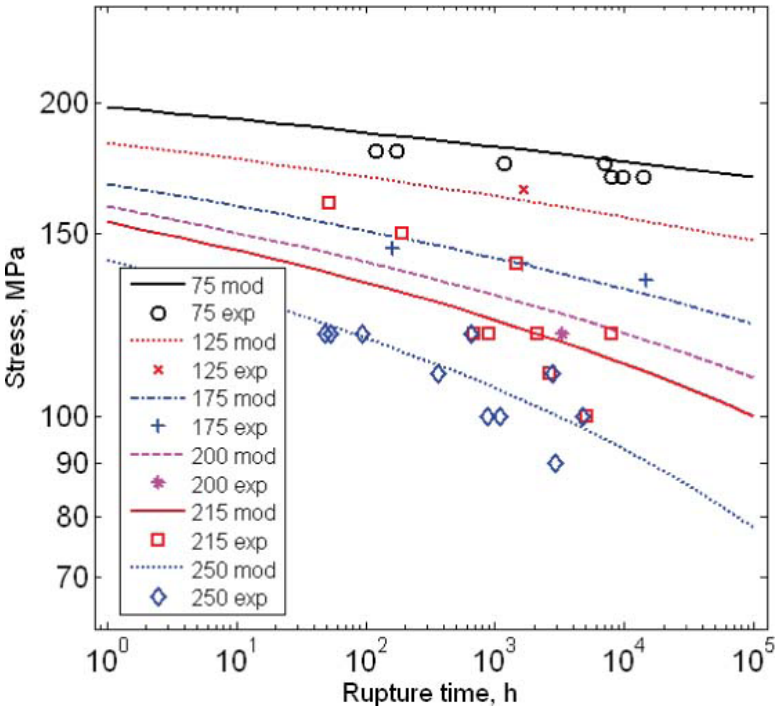

Figure 4-1. *Creep stress versus rupture time for Cu-OFP for temperatures from 75 to 250ºC. The model values are taken from eq. (4-6) and the experimental data from Andersson and Sandström (2009).*

A reasonable description of the uniaxial creep rupture data is found in Figure 4-1, considering the scatter in the experimental values. It should be recalled that there are no fitting parameters involved. It can be concluded that eqs. (4-1) and (4-3) can describe the creep damage development in the uniaxial case.

4.2 Stress distribution

Using the CT-specimen geometry and the loadings from the experiments, stress analysis has been performed using Comsol Multiphysics. The von Mises effective stress along the crack plane is illustrated in Figure 4-2 at 75ºC.

As can be seen from Figure 4-2, the stress close to the crack tip is reduced with increasing time. Thus some stress relaxation due to creep takes place. In Figure 4-3 a comparison is made between the stress states at the four testing temperatures.

The effective stress decreases with increasing temperature, which is natural. In two of the tests (at 20ºC and one at 75ºC) the load was increased at certain intervals. In Figure 4-3, the stress is shown after about half the test time. In that case, considerable creep relaxation has taken place to semi-stationary conditions and the effective stress is not strongly influenced by the initial load level.

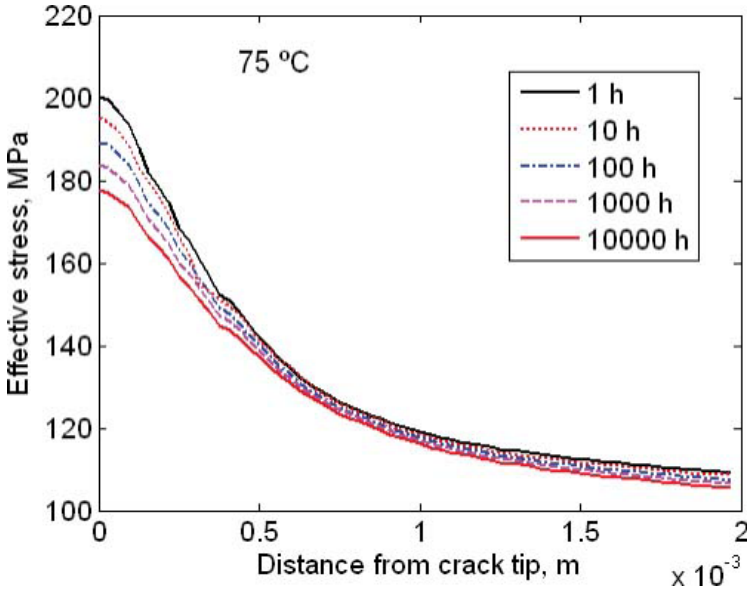

Figure 4-2. *Effective stress versus distance from the crack tip at 75ºC for five times after loading*

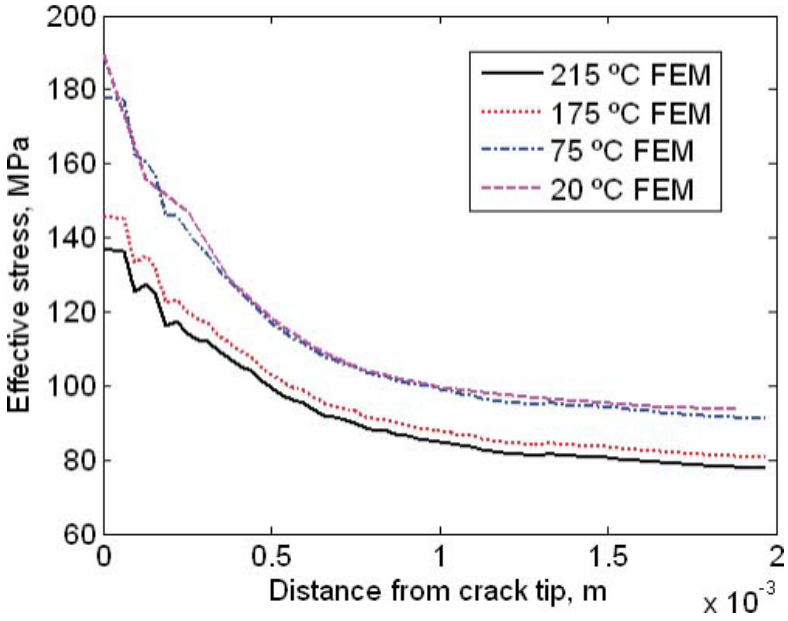

Figure 4-3. *Effective stress versus distance from the crack tip at the temperatures used in the tests.*

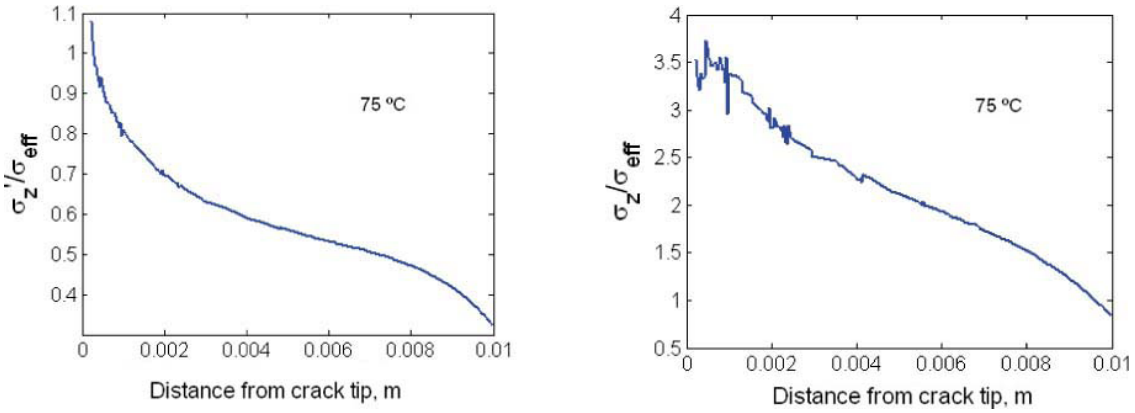

Figure 4-4. *Stress deviator σ_z' and stress σ_z perpendicular to the crack plane.*

The other stress components of interest are the stress deviator σ_z' and stress σ_z perpendicular to the crack plane, cf. eq. (4-4). The stress deviator influences the creep rate and the largest principal stress σ_z the rupture time, cf. eq. (4-1). The ratio σ_z'/σ_e is close to unity near the crack and σ_z/σ_e takes a value of 3 to 3.5. The latter value can seem a bit uncertain due to the scatter in the FEM results, but that is due to the large amount of plastic deformation in Cu-OFP, since the creep stress is much larger than the yield strength. Values of about 3 have been confirmed in studies of materials with little plastic deformation; see for example Holdsworth and Mazza (2009a).

To describe the first part of the stress distribution in Figure 4-2, an exponential function can be used

$$\sigma_e = \sigma_0 e^{-\frac{(x-x_c)}{x_0}} \tag{4-7}$$

where σ_0 is the stress at the crack tip, x the distance in the crack plane from the original crack position, x_c the coordinate of the crack tip, and x_0 a constant. The use of eq. (4-7) is illustrated in Figure 4-5.

The exponential stress distribution in eq. (4-7) is used in section 4.5. The polynomial fit is applied in the crack growth computations to avoid the influence of the local variations in the FEM results.

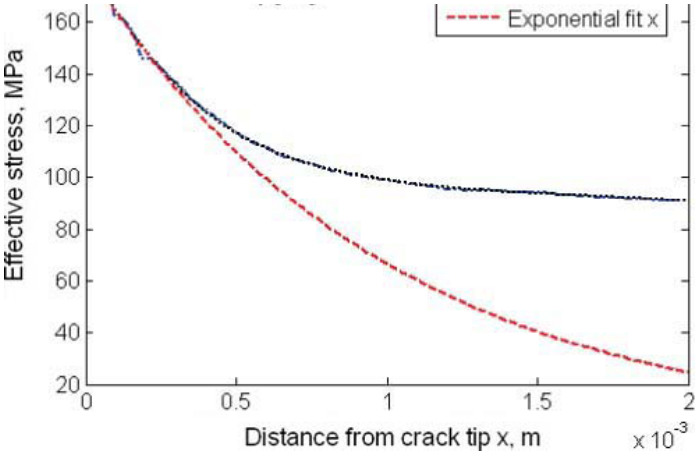

Figure 4-5. *Effective stress in the crack plane as a function of distance from the crack tip. Eq. (4-7) is applied in the exponential fit. 75ºC, 2000 h.*

4.3 Creep damage in front of crack

With the help of the eqs. (4-1), (4-3) and (4-4) and the computed stress distribution, the damage rate behind the crack front can be determined, Figure 4-6.

From Figure 4-6 it is evident that damage rate is rapidly reduced with increasing distance from the crack tip. There is almost an order of magnitude difference in creep damage rate between each temperature level at the crack, and this difference increases with distance from the tip. The initial stress distribution (before crack propagation) is expressed as

$$\boldsymbol{\sigma} = \boldsymbol{\sigma}(x,t) \tag{4-8}$$

The x coordinate is the distance behind the crack tip in the crack plane in the CT specimen. Due to stress relaxation there is also a dependence of the time t, Figure 4-2. Once the crack has started to propagate, the stress distribution is still assumed to follow eq. (4-8) but translated in the x direction

$$\boldsymbol{\sigma} = \boldsymbol{\sigma}(x - x_c(t),t) \tag{4-9}$$

$x_c(t)$ is the position of the crack tip at time t. The damage development in front of the crack tip can be expressed as, eq. (4-1)

$$\dot{\omega} = D\dot{\varepsilon}_c(T, \boldsymbol{\sigma}(x - x_c(t),t))f_{\text{multi}} \tag{4-10}$$

t_0 is the time when the crack starts to propagate. This happens when the integrated damage rate according to eq. (4-10) for $x = 0$ has reached the value one

$$\int_0^{t_0} D\dot{\varepsilon}_{cz}(T, \boldsymbol{\sigma}(0,t)f_{\text{multi}}dt = 1 \tag{4-11}$$

Before the start of the crack propagation $x_c(t) = 0$. From (4-10) the time t_0 can be obtained. Eq. (4-10) can be integrated for each position x in front of the crack. The damage has to be integrated at all positions simultaneously. The reason is that at each time step, the current value of $x_c(t)$ has to be found. $x_c(t)$ is the coordinate where the damage is precisely unity.

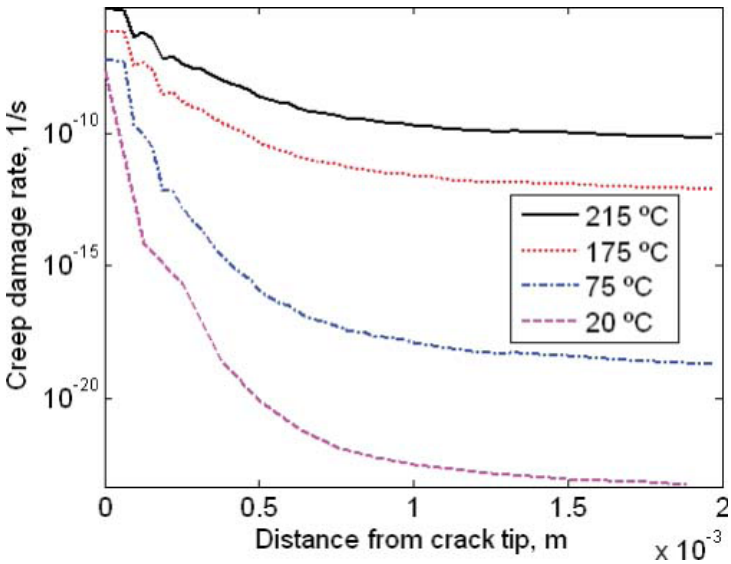

Figure 4-6. *The initial creep damage rate in front of crack according to eq. (4-1) versus the distance from the tip. The factor in (4-2) taking multiaxial effects into account is neglected.*

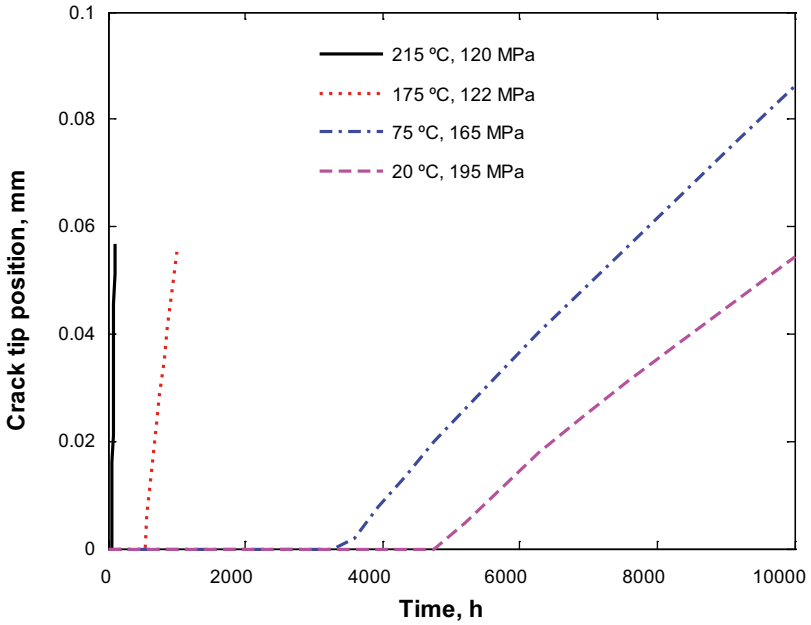

Figure 4-7. *Crack position as a function of time for the test conditions. Multiaxial effects on the damage are neglected (f_{multi}= 1)*

Eq. (4-10) will now be used to predict the crack propagation for the test conditions. The crack position as a function of time is illustrated in Figure 4-7 neglecting multiaxial effects on damage.

For the test durations the total crack propagation is in the range is between 0.05 and 0.09. At 75ºC, the highest reference stress used in the testing 165 MPa is applied in Figure 4-7. At 20ºC the next highest σ_{ref} = 195 MPa is employed because the highest value 205 MPa was only used for a short time. The influence of load changes is not taken into account in Figure 4-7. This would have given even smaller crack propagation. The model values in Figure 4-7 are quite small and are often not even considered as crack initiation, which can be for example set as 0.5 mm crack expansion.

4.4 Multiaxial damage effects

Figure 4-7 can be said to give a good representation of the tests at 20 and 75ºC, where no crack initiation was observed. However, at 175 and 215ºC the crack propagation is dramatically underestimated. In Figure 4-7, full stress relaxation is assumed and not the gradual relaxation in Figure 4-2. This gives additional crack propagation as will be demonstrated below. However, more importantly multiaxial effects on the damage must be considered.

At 75ºC it has been demonstrated that creep strain and rupture for round notched specimens can be described accurately with uniaxial data (Wu et al. 2009). This implies that f_{multi}= 1. This can be assumed to be the case also at 20ºC. At the higher temperatures, data from Kowalewski (2004) will be used. He performed 9 combined tension and torsion creep tests at 250ºC for pure copper with rupture times between 50 and 1500 h. Eq. (4-2a) with γn = 3.26 gives the best fit to his data.

$$f_{\text{multi}} = \left(\frac{\sigma_z}{\sigma_e}\right)^{3.26} \qquad T = 175,\ 215ºC \tag{4-12}$$

From Figure 4-4b, it is evident that the ratio between the maximum principal stress and the effective stress varies between 3.5 and 1 for crack length up to 10 mm. This means that f_{multi} takes values between 60 and 1. This effect is taken into account in Figure 4-8.

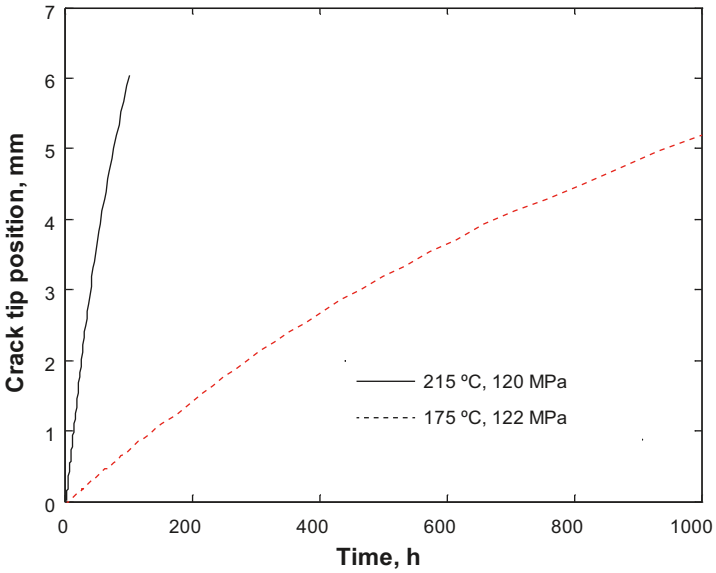

Figure 4-8. *Crack position as a function of time for the test conditions at 175 and 215ºC. Multiaxial effects on damage according eq. (4-12) are taken into account*

For both the tests at 175 and 215ºC the total crack propagation is about 5 mm. In Figure 4-8, the stresses have been assumed to relax to a level corresponding to a significant fraction of the test time, cf. Figure 4-2. It the gradual stress relaxation is taken into account, the initial stresses are higher and the crack propagation larger, see Figure 4-9.

The total crack propagation in this case is 13 mm at both temperatures. Since the constant general stress is lower in Figure 4-8 than in the relaxation stress in Figure 4-9, it is natural that the total crack propagation is larger in the latter case. Even 5 mm crack propagation in Figure 4-9 is more than enough to cause final failure by full separation along the crack plane, since the reduced ligament will increase the stress level substantially and thereby the crack propagation rate and that is not taken into account in the computations. In Figure 4-9 the propagation speed is approximately constant, whereas in Figure 4-9, the speed decreases logarithmically two orders of magnitude. The stress relaxation should in principle be taken into account, but the crack blunting during the initial loading is likely to reduce the effect of the high initial stresses.

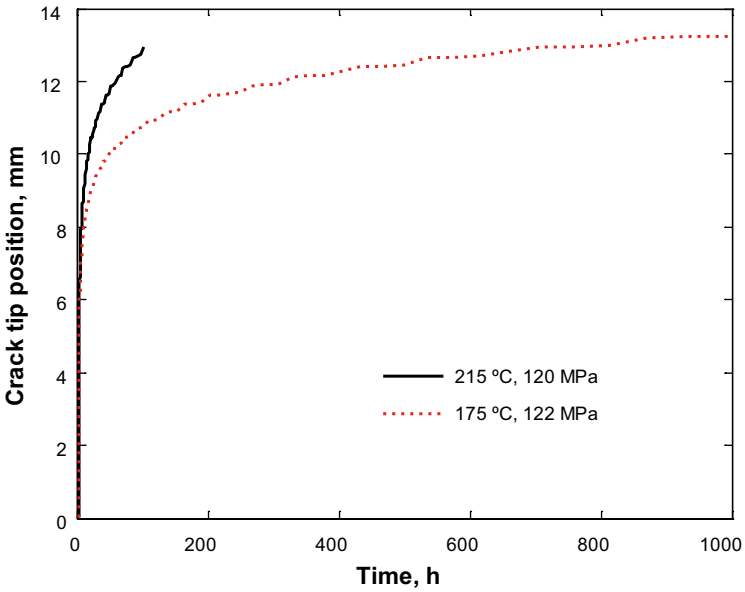

Figure 4-9. *Crack position as a function of time for the test conditions at 175 and 215ºC. Same as Figure 4-8 but including the initial higher stresses*

The propagating stress profile associated with the results in Figure 4-8 is shown in Figure 4-10.

A larger part of the stress profile is illustrated in Figure 4-10 in comparison to Figure 4-2.

4.5 A simplified model for the crack propagation

An analytical model for the crack propagation is derived in Appendix 1. The model is based on three simplifying assumptions: 1) the effective stress decreases exponentially with distance from the crack tip, cf. eq. (4-7), 2) the creep rate can be described by a Norton equation, and 3) σ'_z/σ_e and f_{multi} are approximately constant close to the crack tip. The following expression for the crack propagation speed v is obtained, eq. (A1-14)

$$v = \frac{x_0}{n} D\dot{\varepsilon}_{cz}(T,\sigma_0) f_{\text{multi}} \tag{4-13}$$

In eq. (4-13) the three last factors is the damage rate at the effective stress σ_0 right behind the crack tip, cf. eq. (4-1). Thus, the propagation speed is directly proportional to this damage rate. The larger x_0 and thereby the less steep the stress profile is, cf. eq. (4-7), the higher is the speed. In addition, the speed decreases with increasing Norton exponent n. The values for the propagation speed according to eq. (4-13) are compared to the full model in Table 4-1.

The simplified model gives about factor of 2 to 3 lower values. One reason for this difference is the assumption of a constant Norton exponent. In fact with eq. (4-3) for the creep strain rate, the Norton exponent decreases with decreasing stress away from the crack tip.

Table 4-1. Comparison of propagation speed (m/s) between simplified and full models.

Test temperature, ºC	22	75	175	215
Full model	3.8×10^{-12}	5×10^{-12}	2×10^{-9}	2.0×10^{-8}
Simplified model, eq. (4-13)	1.2×10^{-12}	1.8×10^{-12}	1.1×10^{-9}	1.3×10^{-8}

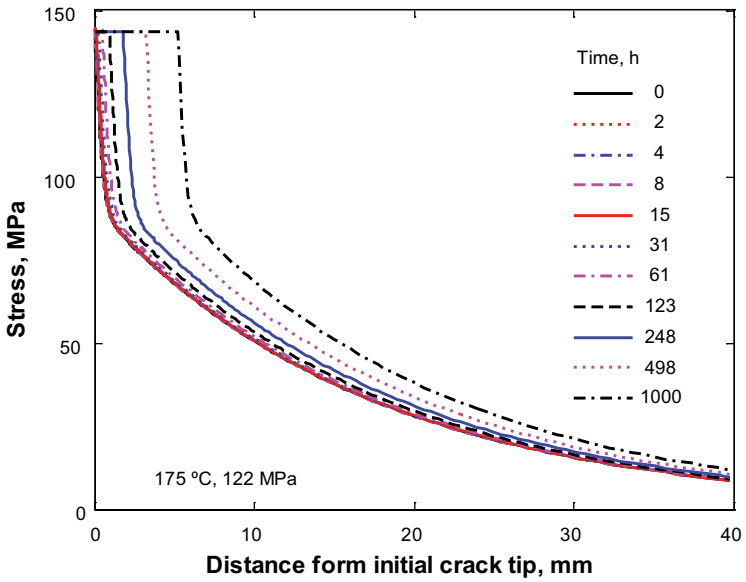

Figure 4-10. *Stress profile in front of propagating crack at different times for the test at 175ºC*

5 Discussion

5.1 Increase in LLD and notch radius during uploading

From Table 3-1, it is seen that load line displacement (LLD) under uploading increases approximately 6–10 mm at applied initial reference stresses and at given temperatures. Such large LLD increase will alter notch radius and will cause plastic deformation/work hardening. Hence, changes in material condition and specimen geometry should be considered when interpreting and applying results. Using dimensions for CT specimen shown in Figure 2-4, assuming no bend on CT specimen during uploading, a rough estimation of maximum notch radius is 0.176 mm at LLD=6 mm and 0.19 mm at LLD=10 mm. Using these estimated values, stress variation at crack tip should be obtained. Using estimated notch radius, local deformations adjacent to crack tip at LLD=6 mm and LLD=10 mm are 17.3% and 26.7%, respectively. This deformation will cause work hardening, and increase in hardness.

5.2 Experiences from CCG testing

Due to good electrical conductivity of copper, the PD recording for all the tests remains almost unchanged with time, see Figures 3-2–3-4, independently whether there is a decrease of cross section area by crack growth. To be able to theoretically calculate change in crack length, *c.f.* eqn. (3-2), an increase in normalised potential drop recordings (V/V_0) is expected. If V/V_0 is unchanged, crack length increase cannot be determined. If the crack length is unknown, stress intensity factor K_I cannot be worked out either, see eqn. (3-1), neither creep fracture parameter C*, which is also related to the crack length (ASTM 2000).

Nevertheless, there are other ways knowing change in crack length and crack tip appearance. One way is to visually monitor and manually measure crack tip opening and growth. In fact, visual observation has been applied in the present investigation, see section 2.3 and Figures 3-1, 3-7 and 3-8. If accuracy of measurement can be ensured, this method should be applicable to obtain crack length extension. One of the advantages with this method is that it is possible to take images of crack and to show dynamic crack growth. In addition, LLD might be utilised to interpret crack growth, since shape of LLD and PD might be analogue. Thirdly, increasing resolution and sensitivity of PD may enhance PD recording, enabling eqn. (3-2).

Because CCG testing in Cu-OFP is very limited and available CCG results in terms of lifetime and crack growth rate are nearly inaccessible, the initial reference stress is difficult to choose to yield reasonable test duration or crack growth rate. To avoid failure during uploading, conservative reference stress is frequently chosen, based to a large extent on uniaxial results. Consequently, forced stress increment must be adopted in order to shorten crack incubation and to initiate crack growth. Stress increment causes instantaneous increase in LLD, or crack growth, see Figures 3-3 and 3-4. On the other hand, stress increment during testing will lead to uncertain test and material condition. Finally, difficulty arises to explain, interpret and apply results. This is also valid for readjustment of loading bar arm level. Readjustment may give rise to an unexpected larger LLD increase, see Figure 3-4. This apparent impact of abrupt stress variation, thereafter crack tip opening and growth cannot be ignored.

5.3 Modelling

Finite element modelling (FEM) has been carried out to determine the stress state behind the crack tip in the CT specimens. The relaxation of the stresses due to creep has also been studied. The stress distributions have been used to predict the creep damage in front of the crack tip. When the damage reached unity the material can no longer support the load and the crack propagates. From the time dependence of the computed damage the crack propagation speed can be predicted. There are two types of multiaxial effects involved in the analysis. The influence of the stress state on the creep rate can accurately be described with Odqvist's equation, which is applied thoughout the analysis.

The multiaxiality also affects the creep rupture and thereby damage. Only empirical relations are available to describe this influence. Two of the most well known relations are given in eq. (4-2). The parameters α and γ are determined by fitting to experiments. The temperature and time dependence of these parameters are unknown in general. At 75ºC creep tests with round notched specimens have been performed (Wu et al. 2009). These results have successfully been modelled assuming $f_{multi} = 1$. Also the crack propagation results at 20 and 75ºC in the present report are consistent with $f_{multi} = 1$. However, at the higher temperatures 175 and 215ºC, a higher value of f_{multi} must be applied. Eq. (4-2a) with $\gamma n = 3.26$ was used after fitting to rupture for combined tension and torsion testing (Kowalewski 2004). This gives a value for f_{multi} that varies from 60 right behind the crack tip down to 1 further away from the tip. In this way the observed crack propagation at 175 and 215ºC could be well described.

It is natural to associate the faster crack propagation at the higher temperature to a more creep brittle condition. This is supported by the post test metallography, which creep cavitation and cracks to a larger extent than at the lower test temperatures. The factor f_{multi} can be interpreted as reduction factor for the multiaxial creep ductility. Ainsworth and Webster suggest that the ductility in plane strain conditions can drop as much as a factor of 50 (Webster and Ainsworth 1994).

The rupture times for CT specimens and uniaxial tests have been compared for steels in recent years. In particular 9%Cr-steels (Holdsworth and Mazza, 2009b) and 1%CrMoV steels (Holdsworth and Mazza 2009b) have been investigated. According to the LICON methodology, the purpose has been to find a testing procedure that give shorter testing times but still preserves the damage that is characteristic of long term testing. In these investigations $f_{multi} \sim 30$ has been found. This is clearly of the same order of magnitude as in the present investigation for Cu-OFP.

It has been suggested for a long time that if the amount of crack propagation is limited, creep design can be based on the reference stress method, see for example Ainsworth (1982). In the reference stress method, conventional stress analysis is used. This implies that it is not necessary to perform full creep strain calculations of components. With the help of the simplified model for creep crack propagation derived in the present paper, it is possible to estimate the risk for dangerous crack expansion if notches or slits are present.

6 Conclusions

Behaviour of creep crack growth (CCG) has been investigated in Cu-OFP parent metal. Five CCG tests using standard compact tension (CT) specimen with notch radius of 0.15 mm have been conducted at 22, 75, 175 and 215°C and modelled. Load line displacement (LLD) and potential drop (PD) have been measured and recorded. Crack tip opening and growth has been visually monitored and recorded for the tests at 22 and 75°C. Pre- and post-test metallography is performed. The following conclusions can be drawn

1. The rupture time in CCG is considerably shorter at the highest test temperatures than that of uniaxial at same stress/reference stress, i.e. by a factor of 65 at 215°C and by several orders of magnitude at 175°C. In contrast, creep crack growth is hardly observed at 22 and 75ºC. Hence, at 175 and 215ºC creep crack growth must be explicitly taken into account in design against creep, whereas this is not required at lower temperatures.
2. At 175 and 215°C, crack does grow by creep about 10 mm before final instantaneous failure. Based on LLD measurement, crack is believed to grow at later stage of test. At 75°C and lower, the crack incubation time increases considerably. Although reference stress has been raised from 135 to 205 MPa and test has run more than 13000 hours, there is hardly any visible crack growth at room temperature. This is also the case for an interrupted test at 75°C, in which reference stress has been raised from 140 to 165 MPa and test has run nearly 5000 hours.
3. Strongly elongated and deformed grains adjacent to crack are observed on the failed specimens tested at 175 and 215°C. Extensive and intergranular creep cavities and microcracks are found several mm around the main crack. Creep damage appears preferably on the mixed grain boundary where small and large grains meet.
4. For the interrupted tests at 22°C (specimen CCG22) and 75°C (specimen CCG75R), hardness adjacent to crack tip has more than doubled because of work hardening, or heavy deformation. This is consistent with large crack tip opening, *e.g.* from 0.3 mm to 1.4 mm for CCG75R and to 3.3 mm for CCG22, respectively. The corresponding true strain at the crack tip is estimated to 10 and 4 for the tests at 22 and 75°C, respectively.
5. LLD under uploading increases approximately 6–10 mm at given test conditions. As a result, notch radius will alter and plastic deformation/work hardening will occur. Hence, changes in material condition and specimen geometry should be considered when interpreting and applying CCG results.
6. Because of good electrical conductivity of copper, the PD recordings for the tests are almost unchanged with time. As a consequence, the crack length cannot be assessed. Nevertheless, there are other ways to monitor crack tip opening and growth, such as visual observation, utilisation and interpretation of LLD, and modified PD method.
7. Stress increment should be constrained, eventually prevented, since this leads to an unsure testing condition. Readjustment of loading bar arm level should also be avoided, if possible, since its impact on abrupt stress variation, thereafter crack tip opening and growth cannot be ignored.
8. Stress analysis has been performed with FEM for the stress state behind the crack tip in the CT specimens. The stress relaxation after loading has been taken into account.
9. The damage in uniaxial creep tests has successfully been described by a basic strain rate model that does not involve any fitting parameters.
10. A crack propagation model has been set up. The crack is assumed to propagate when damage has reached unity in front of the crack. The observed crack propagation can be reproduced by the model provided multiaxial effects are taken into account.

Acknowledgements

This work has been performed at Swerea KIMAB. The financial support from the Swedish Nuclear Fuel and Waste Management Co (SKB) is greatly acknowledged. The SKB is also thanked for providing the test material. The research committee members; Christina Lilja, Håkan Rydén, Magnus Johansson, Sören Claesson, Lars Cederqvist, Nina Leskinen, all from SKB, Henrik Östling, Åsa Martinsson from Swerea KIMAB, Therese Källgren from KTH are thanked for discussions and comments.

References

SKB's (Svensk Kärnbränslehantering AB) publications can be found at www.skb.se/publications.

Ainsworth R A, 1982. The initiation of creep crack growth. International Journal of Solids and Structures, 18, pp 873–881.

Andersson H, 2005. Creep crack propagation in pure copper at 75°C. IM-2005-130, Corrosion and Metals Research Institute, Sweden.

Andersson H C M, Sandström R, 2009. Survey of creep properties of copper intended for nuclear waste disposal. SKB TR-09-32, Svensk Kärnbränslehantering AB.

Andersson H, Seitisleam F, Sandström R, 1999. Influence of phosphorous and sulphur as well as grain size on creep in pure copper. SKB TR-99-39, Svensk Kärnbränslehantering AB.

Andersson H C M, Seitisleam F, Sandström R, 2005. Creep testing of thick-wall copper electron beam and friction stir welds 75, 125 and 175°C. SKB TR-05-08, Svensk Kärnbränslehantering AB.

Andersson H C M, Seitisleam F, Sandström R, 2007. Creep testing and creep loading experiments on friction stir welds in copper at 75°C. SKB TR-07-08, Svensk Kärnbränslehantering AB.

ASTM, 2000. Standard test method for measurement of creep crack growth rates in metals. ASTM E-1457-00, ASTM International.

Auerkari P, Holmström S, Salonen J, 2003. Creep and creep damage in copper under uniaxial/multiaxial loading. SKI Report 2003:29, Swedish Nuclear Power Inspectorate.

Auerkari P, Holmström S, Salonen S, Nenonen P, 2005. Creep performance of OFP copper for the overpack of repository canisters. In: Van Iseghem P (ed). Scientific basis for nuclear waste management XXIX: proceedings of a meeting held in Ghent, Belgium, 12–16 September 2005. Warrendale, PA: Materials Research Society. (Materials Research Society Symposium Proceedings 932), pp 885–892.

Auerkari P, Rantala J, Salonen J, 2009. Effect of defects on low temperature creep of OFP copper. In: Shibli I A, Holdsworth S R (eds). Creep and fracture in high temperature components: proceedings of the 2nd ECCC Conference, Zurich, Switzerland, 21–23 April, 2009, pp 287–297.

Henderson P, Sandström R, 1998. Low temperature creep ductility of OFHC copper. Materials Science and Engineering A, 246, pp 143–150.

Henderson P, Werme L, 1996. Creep testing of copper for radwaste canisters. In: Proceedings of the Euromat 96 – Materials and Nuclear Power, Bournemouth, UK, 21–23 October 1996.

Holdsworth S R, Mazza E, 2009a. Using the results of creep crack incubation tests on CrMoV steel for predicting long time creep rupture properties. International Journal of Pressure Vessels and Piping, 86, pp 838–844.

Holdsworth S R, Mazza E, 2009b. Application of the LICON methodology to a low-alloy ferritic steel. Materials Science and Engineering A, 510–511, pp 95–98.

Johnson H H, 1962. Calibrating the electric potential method for studying slow crack growth. Materials Research and Standards, 5, pp 442–445.

Kowalewski Z L, 2004. Isochronous creep rupture loci for metals under biaxial stress. Journal of Strain Analysis for Engineering Design, 39, pp 581–593.

Lin J, Kowalewski Z L, Cao J, 2005. Creep rupture of copper and aluminium alloy under combined loadings – experiments and their various descriptions. International Journal of Mechanical Sciences, 47, pp 1038–1058.

Miller A G, 1988. Review of limit loads of structures containing defects. International Journal of Pressure Vessels and Piping, 32, pp 197–327.

Raiko H, Sandström R, Rydén H, Johansson M, 2010. Design analysis report for the canister. SKB TR-10-28, Svensk Kärnbränslehantering AB.

Sandström R, Wu R, 2007. Origin of the extra low creep ductility of copper without phosphorus. SKB TR-07-02, Svensk Kärnbränslehantering AB.

Sandström R, Andersson H C M, 2008. Creep in phosphorus alloyed copper during power-law breakdown. Journal of Nuclear Materials, 372, pp 76–88.

Schwalbe K H, Hellman D J, 1981. Application of the electrical potential method to crack length measurements using Johnson's formula. Journal of Testing and Evaluating, 9, pp 218–221.

Seitisleam F, Henderson P, 1997. Creep of copper for nuclear waste containment – results of testing performed in 1996. IM-3506, Corrosion and Metals Research Institute, Sweden.

Webster G A, Ainsworth R A, 1994. High temperature component life assessment. London: Chapman & Hall.

Wu R, Sandström R, 1996. Strain dependence of creep cavity nucleation in low alloy and 12%Cr steels. Materials Science and Technology, 12, pp 405–415.

Wu R, Seitisleam F, Sandström R, 2009. Creep properties of phosphorus alloyed oxygen free copper under multiaxial stress state. SKB R-09-41, Svensk Kärnbränslehantering AB.

Appendix 1

Derivation of a simplified model for creep crack propagation

To obtain an analytical model for the crack propagation we make three simplifying assumptions

1. The effective stress decreases exponentially with distance from the crack tip, cf. eq. (4-7). We know that the part of the stress profile close to the crack tip satisfies this criterion. At 75ºC this is illustrated in Figure 4-5.
2. The creep rate can be described by a Norton equation

$$\dot{\varepsilon}_{cz}(T,\sigma) = \frac{3}{2} B \sigma_e^n \frac{\sigma'_z}{\sigma_e} \tag{A1-1}$$

where B and n are constants.

3. The last ratio in eq. (A1-1) and f_{multi} are approximately constant close to the crack tip

With assumption 1 the stress in the crack plane can be expressed as, cf. eq. (4-7)

$$\sigma_e = \sigma_0 e^{-\frac{x}{x_0}} \qquad t \le t_0 \tag{A1-2}$$

$$\sigma_e = \sigma_0 e^{-\frac{(x - v(t - t_0))}{x_0}} \qquad t > t_0 \tag{A1-3}$$

where σ_0 is the effective stress at the crack tip, x the distance in the crack plane from the original crack position, x_0 a constant, t the time, t_0 the time when the damage has reached unity at the original crack tip, and v the propagation speed of the crack. Eqs. (A1-2) and (A1-3) are applicable before and after the start of the crack propagation, respectively. As a function of distance from the actual crack position, the stress profile remains constant. This type of behaviour is illustrated in Figure 4-10.

Combining eqs (4-1) and (A1-1), the rate of damage development becomes

$$\frac{d\omega}{dt} = D \frac{3}{2} B \sigma_e^n \frac{\sigma'_z}{\sigma_e} f_{multi} \tag{A1-4}$$

At the original crack tip the damage reaches unity at time t_0. Since the damage rate is time independent, t_0 can be obtained from the following expression

$$\omega = D \frac{3}{2} B \sigma_0^n \frac{\sigma'_z}{\sigma_e} f_{multi} t_0 = 1 \tag{A1-5}$$

or

$$t_0 = \frac{1}{D \frac{3}{2} B \sigma_0^n \frac{\sigma'_z}{\sigma_e} f_{multi}} \tag{A1-6}$$

Inserting (A1-6) into (A1-4) simplifies this equation somewhat

$$\frac{d\omega}{dt} = \frac{1}{t_0} \left(\frac{\sigma_e}{\sigma_0}\right)^n \tag{A1-7}$$

Before the crack has started to propagate, the stress profile is given by eq. (A1-2). Applying this expression in (A1-7) gives

$$\frac{d\omega_1}{dt} = \frac{1}{t_0} e^{-\frac{nx}{x_0}} \qquad t \le t_0 \tag{A1-8}$$

The damage before crack propagation is indexed 1. Since this equation is time independent, the amount of damage as a function of time can be obtained directly

$$\omega_1 = \frac{t}{t_0} e^{-\frac{nx}{x_0}} \qquad t \le t_0 \tag{A1-9}$$

After the crack has started to propagate the stress profile is expressed by eq. (A1-3). Inserting this expression into eq. (A1-7) gives

$$\frac{d\omega_2}{dt} = \frac{1}{t_0} e^{-\frac{n(x - v(t-t_0))}{x_0}} \qquad t > t_0 \tag{A1-10}$$

After the start of the crack propagation, the damage contribution is indexed 2. To find the contribution 2, eq. (A1-10) should be integrated from time t_0 to t. This yields

$$\omega_2 = \frac{x_0}{t_0 nv} e^{-\frac{nx}{x_0}} \left(e^{\frac{nv(t-t_0)}{x_0}} - 1 \right) \qquad t > t_0 \tag{A1-11}$$

The total damage for $t \le t_0$ is given by eq. (A1-8). For larger times the contributions from (A1-8) and (A1-11) should be added

$$\omega = \omega_1(t = t_0) + \omega_2 = e^{-\frac{nx}{x_0}} \left[1 + \frac{x_0}{t_0 nv} \left(e^{\frac{nv(t-t_0)}{x_0}} - 1 \right) \right] \qquad t > t_0 \tag{A1-12}$$

The position of the crack tip is

$$x = v(t - t_0) \tag{A1-13}$$

The damage at the crack tip is equal to unity. By using eq. (A1-12) at the crack tip, we find that

$$1 = e^{-\frac{nx}{x_0}} \left[1 + \frac{x_0}{t_0 nv} \left(e^{\frac{nx}{x_0}} - 1 \right) \right] \qquad t > t_0 \tag{A1-14}$$

Rewriting eq. (A1-14), the exponential in the round brackets can be eliminated, and an expression for the propagation speed v is obtained

$$v = \frac{x_0}{nt_0} = \frac{x_0}{n} D\dot{\varepsilon}_{cz}(T, \sigma_0) f_{multi} \tag{A1-15}$$

In (A1-14), eqs. (A1-1) and (A1-6) have been applied.